Annu. Rev. Biochem. 2000. 69:1005–75

STRUCTURE AND FUNCTION OF CYTOCHROME *bc* COMPLEXES

Edward A. Berry
Physical Biosciences Division, Lawrence Berkeley National Laboratory, Berkeley, California, 94720; e-mail: EABerry@LBL.gov

Mariana Guergova-Kuras
Institut de Biologie Physico-Chimique, CNRS, F75005, Paris, France

Li-shar Huang
Physical Biosciences Division, Lawrence Berkeley National Laboratory, Berkeley, California, 94720

Antony R. Crofts
Department of Biochemistry and Center for Biophysics and Computational Biology, University of Illinois at Urbana-Champaign, Urbana, Illinois 61801

Key Words oxidoreductase, respiratory chain, electron transfer, crystallography, membrane protein

■ **Abstract** The cytochrome ***bc*** complexes represent a phylogenetically diverse group of complexes of electron-transferring membrane proteins, most familiarly represented by the mitochondrial and bacterial $\boldsymbol{bc_1}$ complexes and the chloroplast and cyanobacterial $\boldsymbol{b_6f}$ complex. All these complexes couple electron transfer to proton translocation across a closed lipid bilayer membrane, conserving the free energy released by the oxidation-reduction process in the form of an electrochemical proton gradient across the membrane. Recent exciting developments include the application of site-directed mutagenesis to define the role of conserved residues, and the emergence over the past five years of X-ray structures for several mitochondrial complexes, and for two important domains of the $\boldsymbol{b_6f}$ complex.

CONTENTS

0066-4154/00/0707-1005/$14.00

FUNCTION AND DIVERSITY OF CYTOCHROME *bc* COMPLEXES

The complexes of the cytochrome ***bc*** family are related enzymes that developed early in evolution and now carry the major energy fluxes of the biosphere. They couple the redox energy of electron transfer reactions to proton translocation across the membranes of bacteria, mitochondria, and chloroplasts, conserving energy from the oxidation-reduction reactions in a form (the proton electrochemical gradient) that can be used to synthesize ATP, transport solutes, or perform other useful work. These enzymes are multisubunit complexes of integral membrane proteins, requiring detergents to extract them from the membrane and keep them soluble in aqueous solutions.

We will consider as members of that family all protein complexes that have cytochrome ***b*** and iron-sulfur proteins (ISP) with significant sequence homology to those of the mitochondrial $\boldsymbol{bc_1}$ complex. Most members of the family also include an attached ***c***-type cytochrome such as cytochrome $\boldsymbol{c_1}$ or ***f***, but these need not be evolutionarily related between the subfamilies. Indeed the primitive form seems to have been a cyt ***b***–ISP complex. Many cytochrome ***bc*** complexes also have one or more other subunits with no prosthetic groups. The subunit composition of different ***bc*** complexes will be discussed further in a later section, with reference to the known structures of the mitochondrial and chloroplast enzymes and the phylogenetic distribution of the family.

The cytochrome ***b*** has two B-type hemes, which are often quite different in spectral and redox properties. The ISP contains an Fe_2S_2 cluster with an unusually high redox midpoint potential. The cytochrome ***bc*** complexes catalyze electron transfer from a hydroquinone (ubiquinol, menaquinol, or plastoquinol) to a small soluble redox protein such as cytochrome ***c*** or plastocyanin. If the acceptor is a cytochrome then the Enzyme Commission number for the activity is EC 1.10.2.2; if it is plastocyanin it is EC 1.10.99.1. Since some cyanobacterial and algal $\boldsymbol{b_6f}$ complexes can use either acceptor, the same enzyme has in principle two EC numbers.

The cytochrome $\boldsymbol{bc_1}$ complex, or ubiquinol–cytochrome ***c*** oxidoreductase, is present in mitochondria and in proteobacteria of the alpha subdivision. In some cases it functions in electron transfer chains for both respiration and cyclic photosynthesis in the same organism. Menaquinone rather than ubiquinone is the natural substrate in some organisms. The $\boldsymbol{b_6f}$ complex, plastoquinol-plastocyanin oxidoreductase, functions in the electron transport chains of oxygen-evolving photosynthesis in chloroplasts and cyanobacteria. In some cyanobacteria and algal chloroplasts cytochrome $\boldsymbol{c_6}$ is an alternative electron acceptor.

The $\boldsymbol{b_6f}$ complexes have a shorter cytochrome ***b*** corresponding to the N-terminal heme-bearing part of mitochondrial cytochrome ***b***, while sequences similar to the C-terminal part are present in a separate subunit IV. The ***c***-type cytochrome is cytochrome ***f***, which is structurally unrelated to cytochrome $\boldsymbol{c_1}$. Common features and distinguishing differences of the different ***bc*** complexes will be discussed in

a later section. Most of the characterization and structural and functional studies reviewed here have been performed with the mitochondrial and α proteobacterial $\boldsymbol{bc_1}$ complexes and the chloroplast $\boldsymbol{b_6f}$ complex.

The history of studies of the mitochondrial $\boldsymbol{bc_1}$ complex and other mitochondrial membrane components, from the discovery by MacMunn (1) and rediscovery by Keilin (2) of cytochromes, through the functional and biochemical isolation of the four respiratory complexes, including the cytochrome $\boldsymbol{bc_1}$ complex (complex III), has been reviewed in monographs by Wainio (3) and Nicholls (4). Later reviews appeared periodically as the $\boldsymbol{bc_1}$ complex and a few other cytochrome ***bc*** complexes began to be characterized physically and functionally, and as homology between the mitochondrial $\boldsymbol{bc_1}$ complex and the ***bc*** complexes of photosynthetic bacteria and the chloroplast and cyanobacterial $\boldsymbol{b_6f}$ complex was recognized, leading to the current picture of the complexes (5–13).

Now there is a great proliferation of gene sequence information from a wide range of organisms, owing to vastly improved sequencing techniques and various genome sequencing projects. Members of the ***bc*** complex family can be identified in all three kingdoms of life without measuring activity or recording a spectrum, and it is possible to speculate about the evolution of the complex from a very early ancestor. In the last few years atomic models of several vertebrate mitochondrial complexes have become available (14–16), that of the fungal complex is forthcoming, and bacterial and chloroplast complex structures are expected shortly. It is an exciting time to be writing a review of these complexes.

The entire field of ***bc*** complexes can no longer be covered exhaustively in a review of this size. To meet size and time constraints, the authors have elected to cover areas they feel more qualified to discuss or find personally more interesting, or that are more closely related to their own work. Thus many important contributions within the last decade have been glossed over or ignored entirely, and this is not intended to be a judgment on the value of these works.

PURIFICATION OF *bc* COMPLEXES

The first protocols for purification of mitochondrial cytochrome $\boldsymbol{bc_1}$ complexes involved salt fractionation in bile detergents. These procedures start with a centrifugal red-green split in which cytochrome oxidase is in a pellet and complexes I, II, and III are selectively extracted. This separation is very effective, but separating complex III from complexes I and II is less efficient and requires multiple steps of fractionation. Rieske and coworkers purified the cytochrome $\boldsymbol{bc_1}$ (complex III) either from the supernatant of the red-green split (17), from purified complexes I + III (NADH:cytochrome ***c*** reductase) (18), or from a side fraction from the preparation of complexes I + III (19, 20) by salt fractionation with $(NH_4)_2SO_4$ in cholate detergent. Later Yu et al (21) purified complex III ($\boldsymbol{bc_1}$ complex III) from pure complex II + III (succinate:cytochrome ***c*** reductase, or SCR). SCR was extracted at pH 10.5, which solubilized a two-subunit succinate dehydrogenase. The

pellet was fractionated in deoxycholate with $(NH_4)_2SO4$ (21) or NH_4OAc (22) to remove the small subunits of complex II. A variant of the latter method was used for preparing the $\boldsymbol{bc_1}$ complex for crystallization in the tetragonal space group from which the structure 1QCR was determined (23, 24).

Neither of these procedures uses any chromatographic steps; in fact Rieske (20) states that complex III is denatured by "adsorption to surfaces (e.g. withdrawal of the enzyme into a capillary pipette or passage of the enzyme through a chromatographic column)." However, von Jagow and coworkers developed a chromatographic purification on hydroxyapatite starting with a Triton X-100 detergent extract of mitochondria, treated with antimycin (25) or not (26). An updated description of this method has appeared (27). Musatov & Robinson (28) developed a procedure that combines the selective Triton extraction of the Schagger method with the Rieske salt fractionation in bile salts.

Another chromatographic procedure was developed by Weiss and coworkers (29) for the *Neurospora* mitochondrial $\boldsymbol{bc_1}$ complex, also involving solubilization in Triton X-100 but using affinity chromatography on immobilized cytochrome ***c***, ion exchange, and size exclusion chromatography instead of hydroxyapatite. This procedure was extended to the bovine complex (30), using yeast cytochrome ***c*** bound by a free thiol rather than horse cytochrome ***c*** coupled via lysines using cyanogen bromide, and to the plant cytochrome $\boldsymbol{bc_1}$ complex (31).

Trumpower and coworkers developed a chromatographic preparation involving anion exchange chromatography of lauryl maltoside extracts. The procedure has since been applied for isolation of cytochrome $\boldsymbol{bc_1}$ complexes from α proteobacteria (32–38), firmicutes (39, 40), and from mitochondria of animals (34), plants (41), fungi (34), *Chlorophyta* (42), and trypanosomes (EA Berry, L-S Huang, HA Avila, L Simpson, unpublished data).

For bacterial $\boldsymbol{bc_1}$ complexes, rapid purification using His-tag technologies now provides an attractive alternative (43, 44).

Purification of Chloroplast and Cyanobacterial bc_1 Complexes

A procedure based on salt fractionation and sucrose density gradient centrifugation of octyl glucoside extracts was introduced by Hauska and coworkers for purification of the chloroplast $\boldsymbol{b_6f}$ complex (45), and was adapted to isolation of the $\boldsymbol{bc_1}$ complex from *Rhodobacter* (46) and the $\boldsymbol{b_6f}$ complex of cyanobacteria (47). Clark & Hind (48) purified spinach $\boldsymbol{b_6f}$ using a column of immobilized cytochrome ***c*** (horse). Chain (49) modified the Hauska preparation to obtain a lipid- and plastoquinone-depleted complex, which could be reactivated. Doyle & Yu (50) replaced the time-consuming and scale-limiting density gradient centrifugation of the Hauska spinach $\boldsymbol{b_6f}$ preparation with calcium phosphate chromatography plus an additional $(NH_4)_2SO_4$ precipitation in cholate detergent. Cramer and coworkers (51) further modified the procedure to allow large-scale, rapid purification of cytochrome $\boldsymbol{b_6f}$ complex.

The b_6f complex from *Chlamydomonas reinhardtii* chloroplasts has been isolated by LeMaire et al (52) and recently by Popot and coworkers (53). The Matsubara group (54) isolated another cyanobacterial b_6f, from *Spirulina*. Recently, Huang et al have purified and crystallized b_6f from the thermophilic cyanobacterium *Mastigocladus laminosus* (55).

Two archaebacterial oxidases, which contain homologs of cytochrome ***b***, have been isolated from *Sulfolobus acidocaldarius* by Lubben and coworkers (56–58). One of them also contains a homolog of the Rieske ISP.

STRUCTURAL STUDIES OF *bc* COMPLEXES

Two-Dimensional Crystals and Electron Microscopy Studies of Cytochrome *bc* Complexes

The first three-dimensional structure information available for cytochrome reductase came from electron microscopic studies of 2-D crystals of the enzyme from *Neurospora* mitochondria by Leonard and coworkers. The crystals were first reported in 1979 (59), and were extensively studied over the next decade. Image data were collected with negative stain and Fourier-transformed to obtain structure factors for filtering and 3-D reconstruction. The resolution extended to 15–20 Å, and the outline of the enzyme was well defined.

The two-dimensional crystals were in the space group P21212, with rows of dimers with alternating up-down orientation spaced by 111 Å along the diagonals of the unit cell and rows of same-orientation dimers spaced by 137 Å along the ***a*** axis and 174 Å along the ***b*** axis.

A subcomplex lacking the core peptides was also crystallized and analyzed, and from comparison of the protein envelope it was possible to show that the core proteins extend into the aqueous phase. (From labeling studies it was known that these proteins were accessible from the matrix side.) (For a review of the results, see 60.)

A later, higher-resolution investigation of the complex with electron diffraction used the purified bovine enzyme reconstituted into tubular helical crystals (61). The complex was inserted in one orientation, with the matrix side inside the tubes, with approximately 11 dimers per turn of the helix. Diffraction data sets were calculated from images, merged, and used to calculate the 3-D structure by helical reconstruction. The intrinsic resolution was estimated at 16 Å. This structure did not generate much discussion, perhaps because the new features observed were still not readily interpretable in terms of protein secondary structure (e.g. number of transmembrane helices), individual subunits could not be identified, and the X-ray structure at higher resolution was expected shortly.

The envelopes of the bc_1 complex determined by electron microscopy and electron crystallography might have been expected to aid in solving the difficult phase problem for 3-D crystals of this large, weakly diffracting protein, but in fact the

first three groups to solve crystal structures each independently used isomorphous replacement to solve the phase problem.

Vermeglio and coworkers (62) purified native tubular photosynthetic membranes from a strain of *Rhodobacter sphaeroides* deficient in light-harvesting complex LH2 and found the membrane proteins to be present in a crystalline array. A projection map was calculated from negative stained images. The monoclinic unit cell was interpreted as containing two reaction centers, and 2 rings of 12 light-harvesting complex LH1 α,β-dimers. The features attributed to these proteins accounted for most of the density. If the stoichiometry of the components was that of a supercomplex (as found in the starting membrane preparation), a monomer of the $\boldsymbol{bc_1}$ complex would have been expected in the unit cell. However, it is not obvious that the unaccounted density could accommodate a $\boldsymbol{bc_1}$ complex monomer. Certainly the $\boldsymbol{bc_1}$ complex could not be arranged in dimers, as the mitochondrial and chloroplast ***bc*** complexes are, because a single monomer per unit cell implies the same orientation for all monomers. The dimer observed in the mitochondrial enzyme consists of monomers related by 180° rotation.

Monomer-dimer interconversion in the $\boldsymbol{b_6f}$ complex has been studied by various techniques including single-particle electron microscopy (63, 64). Like the $\boldsymbol{bc_1}$ complex, cytochrome $\boldsymbol{b_6f}$ is probably a dimer in situ but it can be monomerized under certain conditions.

Mosser and coworkers studied thin 3-D crystals of the $\boldsymbol{b_6f}$ complex and arrived at projection maps based on negative-stained (65) and ice-embedded (66) samples. The former give information about parts extending from the membrane into the medium, while the ice-embedded samples have contrast more uniformly through the membrane. The maps were interpreted in comparison with the structure of the mitochondrial complex, but it has not been possible yet to confirm this interpretation. Very recently, this work has been extended by Breyton (67) to show density changes induced by specific inhibitors that can be interpreted as movement of the Rieske ISP protein. Since there is independent evidence based on electron paramagnetic resonance (EPR) spectroscopy of the ISP cluster in oriented membranes (68) to show that the ISP changes orientation, this supports the interpretation of the projection maps.

Three-Dimensional Crystals of Extrinsic Domains of Cytochrome *bc* Complexes

Martinez and coworkers (69, 70) crystallized the extrinsic domain of cytochrome ***f*** from turnip and solved the structure by multiwavelength anomalous diffraction phasing, giving us the first atomic resolution glimpse of part of a ***bc*** complex [Protein data band (PDB) entries 1CTM, 1HCZ]. Similar constructs have been crystallized from *Chlamydomonas* (71) and the cyanobacterium *Phormidium laminosum* (72), and the structures are available as PDB entries 1CFM and 1CI3.

Link and coworkers (73) crystallized the extrinsic domain of the bovine Rieske ISP. The structure (entry 1RIE) was obtained by Iwata et al (74) to 1.5 Å. Later, the

structure of a similar construct from the chloroplast ISP (entry 1RFS) was solved (75).

The crystallized fragments are small water-soluble proteins, and the crystals in each case diffracted to much higher resolution than any current crystals of the whole complex. These structures will be described with the discussion of individual subunits below.

Three-Dimensional Microcrystals of Mitochondrial Cytochrome bc_1

The Ozawa group was the first to report 3-D crystallization of cytochrome reductase (76). They used cytochrome reductase (complex III) purified by the Rieske ammonium sulfate procedure (20) followed by affinity chromatography on immobilized cytochrome ***c***. Crystallization in the presence of cytochrome ***c*** was achieved by dialyzing against low-ionic-strength medium (10 mM Tris-HCl, pH 7.5) without detergent, followed by freezing and thawing. Although dialysis removed the cholate, no turbidity was observed before freezing and thawing. This was attributed to specifically bound cytochrome ***c***, a hydrophilic protein. After freezing and thawing, crystals were collected by low-speed centrifugation and suspended in 10 mM Tris HCl, pH 7.5. Reddish plates with the largest dimension as much as 50 μm were observed, but the edges tended to be rounded.

To increase the order, the complex was delipidated by hydrophobic chromatography until only about seven phospholipids per cytochrome $\boldsymbol{c_1}$ were present (77). When detergent was dialyzed away at low ionic strength, strongly birefringent needles about 50 μm long and 2 μm thick were formed. Such needles were formed in the presence or absence of cytochrome ***c***. These studies were not pursued further so we do not know much of the nature of these microcrystals.

Macroscopic 3-D Crystals in Needle Habit

Later Gros et al (78) grew needle crystals of cytochrome reductase as long as 0.7 mm. They used cytochrome reductase purified using ammonium sulfate and cholate (the specific procedure was not given). The cholate was exchanged for octyl glucoside or polyoxyethylene detergents by dialysis. The buffer was 100 mM KP_i, pH 6.7. With octyl glucoside (1%) or C_9E_7 (0.35%), crystallization occurred at 20%–30% polyethylene glycol (PEG) 4000 or 6000. With $C_{10}E_7$ (0.35%), crystallization occurred at 20% PEG 6000 or 20%–30% saturated ammonium sulfate. The crystals were not sufficiently large to test X-ray diffraction. The crystallization conditions with octyl glucoside and PEG were taken as a starting point for the crystallization attempts in the lab of one of the authors, with encouraging results that soon led to diffraction-quality crystals.

Diffraction-Quality 3-D Crystals of Vertebrate bc_1 Complex

In the period 1991 to 1992, three groups (79–81) independently published crystallization of the bovine cytochrome $\boldsymbol{bc_1}$ complex with formation of crystals large

enough for X-ray data collection. The three groups had used three different purification protocols, and obtained crystals in three different space groups. Improving the crystals, finding conditions for practical data collection, and solving the phase problem took another five years, so no structural information was available from the crystals until early in 1996 (24). Table 1 includes vital statistics of 3-D crystals that have been used in X-ray crystallographic studies of the mitochondrial $\boldsymbol{bc_1}$ complexes. The crystals that have actually provided structures have either one or two monomers in the asymmetric unit. Type 3 crystals probably have four monomers in the asymmetric unit. The presence of more than one monomer in the asymmetric unit (i.e. noncrystallographic symmetry) is generally useful for structure determination. If there is asymmetry in the $\boldsymbol{bc_1}$ dimer, such crystals give the possibility of obtaining independent structures for each monomer. To the extent that the monomers are identical, noncrystallographic restraints can be used in refinement so that the number of parameters being refined is essentially the number required to define a monomer, while the large asymmetric unit results in a finer sampling of the molecular transform and thus a greater number of unique reflections constituting a data set to a given resolution. The result is an improvement in the ratio of data to parameters and a more overdetermined refinement problem.

The last column of Table 1 gives the packing parameter V_m defined by Matthews (82), the volume of the unit cell divided by the molecular mass of the unit cell contents. The values are all around 4 $Å^3$ per dalton (Da), which is rather loose packing by standards of soluble proteins, and corresponds to a solvent content of 70%. Note, however, that lipids and detergent were not included in the molecular mass, and so are considered to be solvent in this treatment. It can be seen that most of the crystals actually providing X-ray structures had packing coefficients less than 4, and also that the cell volume of a given crystal form can vary considerably with composition of the mother liquor and temperature of data collection.

Tetragonal Crystals of Bovine bc_1 Complex from Stillwater/Dallas

In 1991, Yu and coworkers published a procedure for growing crystals (79) from the bovine enzyme purified by splitting succinate:cytochrome *c* reductase as described (22). The final pellet from NH_4OAc precipitation was redissolved in 50 mM Tris-HCl pH 8.0, 1 mM EDTA, and 0.66 M sucrose, with no detergent other than the cholate carried over in the pellet. This was mixed with an equal volume of precipitating solution, yielding initial concentrations of 25 mM Tris-Cl, 0.33 M sucrose, 0.25 M NaCl, 6% PEG 4000, 0.04% decanoyl N-methylglucamide (DMG), 1.8% heptanetriol, and 0.05% NaN_3. This was subjected to vapor diffusion against a reservoir of higher osmolarity. Crystals grew in 2–4 weeks. Square or octagonal plates were formed, with crystals as large as $4 \times 2 \times 1$ mm. In later experiments (83), the Tris buffer was replaced with 50 mM 2-(*N*-morpholino)ethanesulfonic acid (MES) buffer pH 7.0. These crystals diffracted to 4.5 Å, but a note was added in proof that crystals diffracting to 3.5 Å had been obtained.

TABLE 1 Parameters of different forms of mitochondrial cytochrome bc_1 crystals

Crystal form (Reference)	Space group	#AU/ cell[a]	Mono/ AU[b]	Temp.[c]	Unit cell (Å, degrees)						Volume[d] (10^6 Å^3)		V_m^e (Å^3/Da)
					a	b	c	α	β	γ	UC	AU	
1. I tetragonal (79)	$I4_122$	16	1										
Yu et al (83)				amb.	157	157	590	90±	90±	90±	14.54	0.91	3.74
Lee et al (95)				cryo.	153	153	597	90±	90±	90±	13.98	0.87	3.59
1QCR (14)				cryo.	154	154	598	90±	90±	90±	14.08	0.88	3.62
2. P tetragonal	$P4_{1(3)}$	4	(4)										
Kawamoto et al (88)				amb.	190	190	445	90±	90±	90±	16.06	4.02	4.13
3. Monoclinic 1	$P2_1$	2	(4)										
Kubota et al (80)				amb.	196	179	253	90±	97±	90±	8.81	4.41	4.53
4. Monoclinic 2	$P2_1$	2	2										
Berry et al[f] (90)				amb.	118	178	200	90±	106±	90±	4.03	2.02	4.15
5. Hexagonal 1 (81)	$P6_522$	12	1										
Low glycerol				amb.	217	217	378	90±	90±	120±	15.41	1.28	5.28
High glycerol (81)				amb.	212	212	352	90±	90±	120±	13.70	1.14	4.69
Glycerol, cryo				cryo.	212	212	343	90±	90±	120±	13.35	1.11	4.57
1BE3 (16)				cryo.	211	211	339	90±	90±	120±	13.07	1.09	4.48
Rabbit bc_1				amb.	212	212	354	90±	90±	120±	13.90	1.16	4.76

6. Hexagonal 2 (88)	$P6_5$	6	2										
Kawamoto et al (88)				amb.	131	131	720	90±	90±	120±	10.70	1.78	3.67
Berry et al (90)				amb.	134	134	752	90±	90±	120±	11.69	1.95	4.01
Murakami et al (89)				amb.	128	128	716	90±	90±	120±	10.16	1.69	3.48
1BGY (16)				cryo.	130	130	721	90±	90±	120±	10.55	1.76	3.62
7. Orthorhombic (15)	$2_12_12_1$	4	2										
Chicken				amb.	179	187	244	90±	90±	90±	8.17	2.04	4.20
1BCC (15)				cryo.	170	183	241	90±	90±	90±	7.50	1.87	3.85
3BCC (15)				cryo.	173	180	238	90±	90±	90±	7.41	1.85	3.81

[a]#AU/cell, the number of asymmetric units in the unit cell for this space group.

[b]Mono/AU, the number of monomers in the asymmetric unit (uncertain in the case of crystals 2 and 3, which have not been phased).

[c]Temperature of data collection: cryo. means 70–100 K, amb. means 275–298 K.

[d]Volume: volume of the unit cell (UC) and asymmetric unit (AU) in cubic angstroms divided by 10^6.

[e]Packing parameter (82), cubic angstroms per dalton, based on number of monomers per asymmetric unit and a molecular weight of 243,252 for the monomer (104). Ignores lipid and detergent.

[f]The monoclinic beef crystals were mistakenly reported as centered orthorhombic ($C222_1$) in Reference 90.

The preliminary structure was reported at meetings in 1996 (23, 24), and the full report appeared in 1997 (14). The space group was $I4_122$, with cell dimensions 153.5, 153.5, 597.7 Å (1QCR). While the long ***c*** axis would appear to make data collection difficult because of spot overlap, this is the body-centered lattice with systematic extinctions for general reflections with Miller indices $h + k + l \neq 2n$. The primitive lattice is smaller, and the closest spacing corresponds to the reciprocal of only half the body-centered ***c*** axis or 299 Å, which is not problematic with a well-collimated X-ray beam.

These crystals have a monomer in the asymmetric unit, and the packing in the a, b plane is essentially the same as in the membrane crystals from *Neurospora crassa* (60), with rows of dimers with alternating up-down orientation spaced by 109 Å along the cell diagonals, and rows of dimers with the same orientation spaced by 154 Å along the a or b edges. Layers of such membranes are stacked with each layer rotated 90° relative to the membrane below it, about a fourfold axis 1/4 along the diagonals. This puts each dimer in one membrane in register with a center between four dimers in the membranes above and below. Four such layers complete the unit cell in the C direction, as the fifth has the same orientation as the first. This interaction with the 90°-rotated layers above and below squares up the a-b projection of the unit cell, which was rectangular in the *Neurospora* 2-D crystals. Most of the crystal contacts within one layer involve the two largest subunits, projecting alternately on either side of the membrane layer. The intermembrane P-side protrusion is poorly ordered and does not appear to make any crystal contacts.

All iron centers were located by anomalous scattering as well as by peaks in the conventional electron density (14, 23). The anomalous peaks corresponding to the ISP cluster were weaker than those of the cytochromes, despite the presence of two irons in each cluster, presumably as a result of poor order. Nearly complete models for the subunits on the matrix side of the membrane and for cytochrome ***b*** were built. Transmembrane helices belonging to cytochrome $\boldsymbol{c_1}$, the ISP, and subunit 7 were assigned, and two other helices corresponding to subunits 10 and 11 were built but not assigned. Electron density for the protein in the extrinsic domain of the Rieske protein was not interpretable, so only the matrix side and transmembrane helix were constructed. Several fragments with unassigned sequence were built in the region of the extrinsic domain of cytochrome $\boldsymbol{c_1}$ and the hinge protein. Binding sites for the inhibitors antimycin, myxothiazol, methoxy-acrylate-stilbene (MOA), undecyl hydroxydioxo benzothiazole (UHDBT), and stigmatellin were presented (14, 84).

Further studies by the Deisenhofer group (84) showed that inhibitors at the Q_o site (discussed below) affected the order of the Rieske ISP. The inhibitors stigmatellin and UHDBT, which were believed to interact with the ISP cluster because of effects on its midpoint potential and EPR spectrum (85, 86), improved the order of the ISP extrinsic domain. The MOA inhibitors, which have less effect on the midpoint potential, resulted in more disorder of the ISP.

Monoclinic, Tetragonal, and Hexagonal Crystals of Bovine bc_1 Complex from Osaka/Himeji

The Matsubara group (80) in Osaka published crystallization of the $\boldsymbol{bc_1}$ complex soon after the report from the Yu lab. They used the Rieske method (20) with a final step of polyethylene glycol precipitation from histidine-sucrose buffer with sucrose monolaurate detergent. The crystals were monoclinic with unit cell dimensions $196 \times 179 \times 253$ Å and unique angle $\beta = 97^\circ$. They diffracted synchrotron radiation ($\lambda = 1.04$ Å) to a resolution of 7.5 Å at room temperature. A Matthew coefficient of 4.4 Å^3/Da was calculated assuming two dimers in the asymmetric unit. More details about factors affecting the crystallization were published (87) in a paper discussing crystallization of large transmembraneous protein complexes, such as the $\boldsymbol{bc_1}$ complex and cytochrome oxidase.

Two new crystal forms were reported in 1994 (88) and in the 1992 and 1993 activity reports from the National Lab for High-Energy Physics (nicknamed the Photon Factory), Tsukuba, Japan. Hexagonal prism crystals were indexed on a hexagonal lattice with a long c axis (720 Å) and a sixfold screw axis along c. Assuming a dimer in the asymmetric unit gave a Matthew coefficient of 3.9 Å^3/Da. Inclusion of Zn^{2+} ions at 1–4 mM improved the reproducibility of crystallization, without significantly affecting cell parameters. This crystal form has been obtained by other groups (below) and eventually provided the structure deposited as 3BGY. Note that there are no systematic extinctions for general reflections in this space group, so the 720-Å c axis results in very closely spaced diffraction spots. Collection and processing of an accurate data set to 3.0 Å (16) is a noteworthy achievement.

Crystallization as a final purification step was judged to remove some polypeptides, and the redissolved microcrystalline material crystallized in tetragonal space group with the longest axis c = 445 Å, P41 or P43 symmetry, and $V_m = 4.4$ Å^3/Da assuming two dimers in the asymmetric unit. The hexagonal crystals grown in the presence of Zn^{2+} and the tetragonal crystals diffracted X rays to about 6.5 Å.

The Matsubara group was involved in the electron microscopy study (61) mentioned above. After the retirement of Matsubara, the focus of the work shifted to the Yoshikawa group at the Himeiji Institute. The hexagonal crystals were greatly improved, giving diffraction to 2.8 Å (89), but no structure based on X-ray diffraction has been reported yet.

Various Crystal Forms Including Orthorhombic Chicken bc_1 Crystals from Berkeley

Berry and coworkers began crystallization attempts in 1990. They used the dodecyl maltoside–anion exchange method essentially as described for the potato complex (41). Starting conditions were designed based on the results of Gros et al (78), and the initial crystals were large needles apparently growing out of phase-separated spheres of protein-rich phase. They diffracted X rays weakly and showed symmetry

P61 or P65, with the c axis ~700 nm (EA Berry & L-S Huang, unpublished results). Attempts to improve led to lower ionic strength and pH, and occasionally yielded small hexagonal bipyramids. Bipyramids could be produced routinely by microseeding. These crystals were described in 1992 (81). They belonged to the space group $P6_122$ or $P6_522$. They diffracted to 4.6 Å using synchrotron radiation recorded on X-ray film, and 3.8 Å with imaging plate detector (90).

Two new crystal forms were reported in 1995 (90). The initial needle crystals were improved in size and shape to give uniform or tapered hexagonal rods. Diffraction was not significantly improved, but unit cell parameters were determined: a = b = 134 Å, c = 752 Å, close to those of the hexagonal form reported earlier by the Japanese group (88). These crystals formed initially when seeding failed or was omitted, and dissolved later when either hexagonal bipyramids or a new form of crystal began to grow. The hexagonal rods thus seemed to serve as a protein reservoir, keeping the protein native until a crystal with lower solubility could nucleate and compete for the protein.

The new crystal form was indexed on a face-centered orthorhombic lattice, and assigned the space group $C222_1$ based on systematic absences along the 0 0 L axis. Later attempts to merge the data in this space group showed that the symmetry elements implied by this assignment were not all present, and it was reassigned as primitive monoclinic ($P2_1$) with cell constants given in Table 1. The orthorhombic shape of the centered cell must be coincidental, as it is not required by the symmetry. Like the hexagonal bipyramids, the monoclinic crystals diffracted to about 3.75 Å.

Later, the chicken complex was crystallized in space group $P2_12_12_1$, diffracting to 3.0 Å. These crystals could be cryo-cooled (after increasing the glycerol concentration in the mother liquor to 250 ml/liter or higher), with no loss of resolution and slight increase in mosaicity. These crystals were phased by multiple isomorphous replacement, and electron density of the $\boldsymbol{bc_1}$ dimer in these crystals was used as a search model (91) to phase the other crystal forms by molecular replacement. The molecular replacement procedure determined the enantiomorph of the hexagonal bipyramids to be $P6_522$, and the resulting phases allowed location of heavy atom sites in several derivatives of these crystals for independent isomorphous phases. The same dimer arrangement was present in all crystal forms. In the chicken orthorhombic and beef monoclinic crystals, the dimer axis represented noncrystallographic symmetry, providing two independent views of the structure and permitting questions about asymmetry of the dimer. No significant asymmetry has been noted to date.

In the hexagonal bipyramids from beef or rabbit, the dimer axis fell on a crystallographic twofold axis, so that the asymmetric unit contained only a monomer. Together these four crystal forms provided six crystallographically independent views of the structure. While the distances between heme irons were the same in all six models, the distance from the ISP cluster to the heme irons varied slightly (91) and were all different from the corresponding distances in the tetragonal crystals of the Texas/Oklahoma group (23). When the complex was treated with the inhibitor stigmatellin at slightly more than stoichiometric concentration before

crystallization (15), the position of the ISP cluster was the same as in the tetragonal crystals. Functional implications of the mobility of the Rieske protein will be discussed in a later section.

The orthorhombic chicken crystals were the best ordered of the four forms and so were chosen for refinement of the model. The protein sequence was available only for cytochrome ***b***, so the other subunits were built using the beef sequence or a consensus sequence obtained by choosing the most frequently occurring amino acid among vertebrate sequences at each residue. Three structures from the orthorhombic chicken crystals were deposited in the Protein Database. Entry 1BCC is the native structure with a model for quinone at the Q_i site, 2BCC is from crystals with stigmatellin bound, and 3BCC has stigmatellin and antimycin bound. Entries 1BCC and 3BCC were submitted first, in March 1998. During subsequent refinement it became clear that the orientation of the stigmatellin molecule and glutamate 272, a key residue involved in its binding, were incorrect. The corrected model was included in entry 2BCC, submitted in October 1998. The quinone bound at the Q_i site and stigmatellin at the Q_o site were further described in two papers and a review in 1999 (92–94).

Tetragonal and Two Hexagonal Crystal Forms of Bovine bc_1 from Berkeley/Uppsala

Lee et al (95) grew crystals of the same form used by the Texas/Oklahoma group, and developed a procedure for cryo-cooling the crystals without loss of diffraction. Later, together with the Iwata group in Uppsala (16), they published structures of the bovine complex from much improved and cryo-cooled crystals of the hexagonal bipyramids ($P6_522$) and the hexagonal rods. They determined the latter to be the $P6_5$ enantiomer with a dimer in the asymmetric unit. In the cryo-cooled bipyramids the ISP cluster was closer to the heme of cytochrome $\boldsymbol{c_1}$ than in any other crystal form, implying a hydrogen bond from the cluster-liganding H161 of the Rieske protein to a heme propionate (16). In the $P6_5$ crystals the ISP was found in an intermediate position in one monomer, and was disordered in the other. These structures were the first to assign sequence to the C-terminal end of subunit 9, the presequence of the ISP that is retained in the complex (discussed below). Further details about conformational changes of the ISP, including both movement of the extrinsic domain and a change within the extrinsic domain, were provided in a report from the Iwata group the next year (96).

Higher-Resolution Structure of the Yeast bc_1 Complex

Hunte et al presented crystallization of the yeast $\boldsymbol{bc_1}$ complex in the presence of stigmatellin and a monoclonal antibody Fv fragment (97). It is our understanding from presentations at meetings (98) that a model for this complex is currently being refined at 2.3-Å resolution. However, nothing has been published or submitted to the PDB as this review is submitted.

Comparison of the Different X-Ray Structures

Statistics on data reduction and refinement from the six structures of vertebrate mitochondrial cytochrome $\boldsymbol{bc_1}$ that are available at this writing are presented in Table 2. Aside from the different positions of the ISP extrinsic domain, and excepting subunit 9, there were no major differences between the six structures. Berry et al (93) pointed out one difference in cytochrome $\boldsymbol{c_1}$, in that the region between residues 68 and 85 was modeled as two strands of antiparallel β sheet in the chicken structure, with the turn at conserved G78 making contact with cytochrome $\boldsymbol{c_1}$ in the other monomer. The beef structures 1BE3 and 1BGY modeled this as an α helix, with no dimer contact. The region is poorly ordered in all three crystals, however, and the difference is more likely due to a modeling error than to a species or crystal-packing difference.

The different structures are most reliable in different regions of the dimer, and it seems that no one structure is markedly better than the others are. In studying a particular region or feature it is probably best to examine it in all the structures, and if differences are noted, try to decide which is more accurate in that region. Unfortunately, the atomic temperature factors in the submitted coordinates files are not very useful here, because at least in the case of the originally submitted structures from Berkeley and Uppsala (1BCC, 3BCC, 1BE3, and 3BGY), the models were refined against datasets that had the overall B modified by scaling against a less-ordered crystal (E Berry, unpublished information) or sharpening to enhance map features (S Iwata, personal communication). It is to be hoped this will be corrected in future updates. Overall B-factors from refinement of the Berkeley structures against reprocessed datasets in which the overall B-factor had not been modified are available in Reference (99), and the resulting coordinates will be submitted in the first update of the PDB files. In the meantime, the atomic B-factors in the deposited structures can be used for determining which parts of the molecule are well ordered, but not for comparison with other structures.

None of the models is quite complete. Even if all subunits are present, N or C termini are missing from some of them. It is not unusual for termini and flexible loops to be disordered in protein crystals. Table 3 lists the protein segments present in each structure. One difference not evident from this table is that the structure 1QCR contains only α carbons of each protein residue, and only one of the three hemes. Presumably, side chains were present during the reported refinement, but were removed before submission. This difference may reflect differences in the philosophy of the investigators as much as the quality of the structures.

To compare the different structures, the backbones of the individual subunits were superimposed to minimize RMS differences between α carbons, and the results for the subunits 1, 2, 3, 6, 7, 9, and 10 are given in Table 4. In most cases the RMS differences were less than 2 Å.

Figure 1 shows a composite dimer of the $\boldsymbol{bc_1}$ complex constructed from the different structures available from the protein database.

TABLE 2 Data refinement statistics for the released structures

	Structure						
	1QCR	**1BCC**	**3BCC**	**2BCC**	**1BCC[a]**	**1BE3**	**3BGY**
Submission date (yymmdd)	970517	980323	980323	980817		980519	980602
Rev date (type)[b]	981014 (0)	980819 (0)	980819 (0)	990827 (2)		990216 (3)	990223 (3)
Resolution	2.7	3.16	3.7	3.50	3.16	3.0	3.0
Atoms refined	14000	31442	31470	31508	31442	16222	31730
Unique reflections	72196	107167	71026	80760	121980	72948	101111
Effective resolution	3.0	3.35	3.85	3.72	3.21	3.22	3.32
R-free	0.37	0.31	0.32	0.32	0.32	0.32	0.36
σ-cutoff	2.0	2.0	2.0	2.0	0.0	0.0	0.0
RMS deviation, bond lengths	NA	0.010	0.011	0.011	0.011	—	—
RMS deviation, bond angles	NA	1.6	1.7	1.9	1.6	—	—
Coordinate error, Å[c]	NA	0.56	0.56	0.30	0.69	0.46[c]	0.62[c]

[a]Refinement using the dataset of 1BCC but using all reflections.

[b]Rev date: date and (type) of last revision, where type 3 implies revised coordinates, lower numbers do not. Type 0 indicates the initial release date.

[c]From cross-validated sigma-A treatment except 1BE3 and 1BGY, which use standard sigma-A treatment.

TABLE 3 Completeness of the cytochrome bc_1 structures

		First and last residue present in submitted structures			
Subunit	**# Residues**	**1QRC**	**1BCC**[*a]	**1BE3**	**1BGY**[*a]
1	446	1–446	4–445	1–446	1–446
2	439	17–439	18–439[*b]	21–439	21–439
3	379 or 380[*c]	2–379	2–380	1–379	1–379
4	241	167–241	1–241	1–241	1–241
5	196	1–196	1–196	1–196	1–196
6	110	8–110	10–109	5–110	5–110
7	81	1–70	2–79	1–81	1–81
8	78	18–48	13–78	15–78	15–78
9	78	21–48	[*d]	46–78	46–78
10	62	4–62	4–60	1–62	1–62
11	56	1–45	[*e]	15–36	15–36
Hemes		1	3	3	3
$[Fe_2S_2]$		1	1	1	1
Lipids			2		
Detergents			1 OG		

[a] These structures have a dimer in the asymmetric unit; completeness of the two monomers was the same except that in 1BGY subunit 5, the ISP, chain E extends only to residue E75.

[b] Residues 289–304 were not built.

[c] 1BCC uses the chicken sequence, which has 380 residues; others use the beef, which has 379.

[d] Sequence not assigned, but chain I includes residues at positions of 65–78 in 1BE3.

[e] Subunit 11 was not seen in the electron density and is not detected by gel electrophoresis of the purified preparation. A peptide of the right mass is detected in some preparations by mass spectroscopy (S Yoshikawa, personal communication).

INDIVIDUAL PROTEIN SUBUNITS OF THE CYTOCHROME bc_1 COMPLEX

Simple Complexes: Three Redox-Active Subunits with No or One Supernumerary Subunits

Some of the α proteobacterial $\boldsymbol{bc_1}$ complexes have been isolated in a fully functional state with only the three subunits containing redox centers: cytochrome $\boldsymbol{b}$, cytochrome $\boldsymbol{c_1}$, and the Rieske iron-sulfur protein. This was the case with the enzymes from *Paracoccus* (33), *Rhodospirillum rubrum* (35), and *Rhodobacter capsulatus* (37).

Rhodobacter sphaeroides has in addition a 15-kDa subunit, which was cloned and sequenced by Usui & Yu (100). It is a relatively hydrophilic protein of 124

TABLE 4 RMS differences (Å) between superimposed backbones of bc_1 subunits

	Subunit									
	1	**2**	**3**	**4**	**5**	**6**	**7**	**8**	**10**	**11**
Residues compared		21–288,	2–379							15–36
	4–445	305–439	(3–380)	1–241	75–196	10–109	2–70	18–48	4–60	
1BCC vs 1BE3	1.699	2.333	1.048	2.764	1.044	1.229	1.211	1.890	0.675	
1BE3 vs 3BGY	0.179	0.110	0.241	0.363	0.916	0.128	0.264	1.797	0.090	0.087
1BE3 vs 1QCR	2.004	0.915	1.803		1.597	0.801	1.148	6.050	9.760	1.769
1QCR vs 1BCC	1.574	2.313	1.978		1.568	1.249	1.049	6.203	9.799	

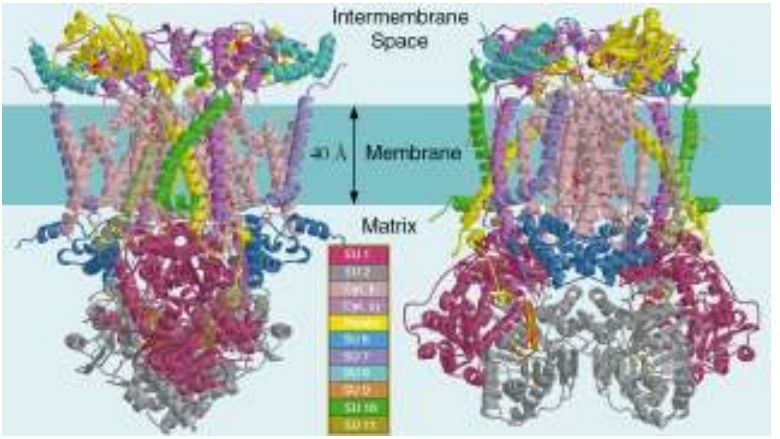

Figure 1 Composite structure of vertebrate mitochondrial cytochrome $\boldsymbol{c_1}$. The *dark horizontal band* indicates the probable membrane position. The *left* and *right* figures are related by a rotation of 90° about the perpendicular to the membrane. Subunits 1, 2, and 11 are from 1QCR; subunits 3–5 and 8 are from 1BCC; 6, 7, 9, and 10 are from 1BE3. The different structures were aligned by superimposing the transmembrane helices of the cytochrome ***b*** dimer before selecting subunits for the composite.

residues, with a transmembrane helix predicted at a hydrophobic stretch between residues 85 and 102. There is no strong similarity with any other sequence in the database. Functional involvement is suggested by resolution and reconstitution experiments (101) and by site-directed mutagenesis (102).

The $\boldsymbol{bc_1}$ complex from *Rhodovulum sulfidophilum* contains, in addition to the three redox-center–bearing subunits, a 6-kDa protein with N-terminal sequence PDNTSNDDVLVPAS (38). This component could be removed by high detergent treatment, but this also removed the Rieske protein, monomerized the complex, and eliminated activity. Thus it is not known whether the 6-kDa protein is required for activity.

Eukaryotic Complexes with 10 or 11 Subunits

The subunit composition has been well characterized and all sequences have been determined for the mitochondrial complexes from three divergent branches of metazoans: beef (103, 104), potato (105), and yeast (106). Ten subunits show sequence similarity between all three complexes, and constitute the entire complexes of yeast and potato. An eleventh subunit present only in the beef complex (subunit 9) turned out to be the leader sequence of the Rieske protein, which is retained within the mature complex (107). For each of the ten conserved subunits from these three mitochondrial sources, Table 5 lists the accession code for the sequence at GenBank, the number of residues, and the molecular weight for the subunits of

TABLE 5 The conserved subunits of beef, yeast, and potato mitochondrial cytochrome bc_1

		Beef cytochrome bc_1			Potato cytochrome bc_1			Yeast cytochrome bc_1		
Subunit	**Name**	**ID**[a]	**#aa**[b]	**MW**[c]	**ID**[a]	**#aa**[b]	**MW**[c]	**ID**[a]	**#aa**[b]	**MW**[c]
1	Core I	CAA42213	(34) 446	53603.6	A48529	(32) 502	56222	P10507	(26) 442	48729
2	Core II	P23004	(14) 439	46524	S51590	(24) 480	51744	P07257	(16)352	38705
3	Cyt ***b***	BAA07016	379	42734	CBPOM	393	44283	CBBY	385	43663
4	Cyt c_1	P00125	(?) 241	27287	S20015	(17) 243	27106	P07143	(61) 248	27771
5	Rieske	P13272	(61) 196	21609	P37841	(78) 212	23141	P08067	(53) 185	20099
6	SU 6	P00129	111	13477	P48502	123	14471	P00128	127	14565
7	QP-C[b]	P13271	82	9720	P46269	72	8317	P08525	94	10975
8	Hinge	P00126	78	9175	P48504	69	7977	BAA09272	147	17257
9	SU 10	P00130	62	7197	P46270	72	8048	P22289	66	7476
10	SU 11	P07552	56	6520	P48505	62	6874	P37299	77	8593

[a] Genbank accession number.

[b] #aa, number of residues. Numbers in parentheses refer to presequences; other numbers refer to mature sequence only.

[c] MW, molecular weight (M_r).

[d] Data are based on nascent protein sequence. There is some evidence that the N-terminal methionine is removed posttranslationally.

TABLE 6 Correlation of the subunits of the ***bc*$_1$** complex from beef, potato, and yeast

Subunit	Name	Beef	Potato	Yeast
1	Core I	1	1	1
2	Core II	2	2	2
3	Cyt ***b***	3	3	3
4	Cyt ***c***	4	4	4
5	Rieske	5	5	5
6		6	6	7
7	QP-C	7	7	8
8	Hinge	8	9	6
9	Cytochrome ***c*$_1$** associated	10	8	9
10	Rieske associated	11	10	10

these three ***bc*** complexes. The molecular mass of a monomer of bovine cytochrome ***bc*$_1$**, calculated from sequences and including the hemes, [Fe_2S_2] cluster, and post-translationally modified residues, is 243,252 Da (104).

The subunits are listed in Table 5 in order of decreasing molecular weight of the bovine protein. The subunits are usually denoted by their position from the top of the gel in the Schagger sodium dodecyl sulfate (SDS) gel system (108) in which mobility closely matches molecular weight. Notice, however, that the relative masses of proteins 8 and 9 are inverted in the potato complex, and protein 8 (the "Hinge" protein) is larger than protein 6 or 7 in the yeast complex. Together with the fact that presequence of the Rieske protein is retained in the beef complex with a molecular weight between that of protein 8 and protein 9, the correspondence given in Table 6 is needed to relate the subunit numbers in the different complexes. For example, the Hinge protein is subunit 8 in the beef complex, subunit 9 in the potato complex, and subunit 6 in the yeast complex. Subunit 11 in the beef complex is subunit 10 in the plant and fungal complexes.

How is the mitochondrial ***bc*$_1$** complex held together? Intersubunit contacts are indicated in Table 7. There are many contacts between the subunits of one monomer (note, however, that assignment of subunits to monomers is somewhat arbitrary, and we have chosen closely packed subunits to constitute our monomer). There are 11 contacts between monomers, 3 of which involve a dimer interface between the same subunit in the 2 monomers. The other 8 involve 4 pairs of asymmetric contacts of each ISP with cytochrome ***c*$_1$** and cytochrome ***b*** of the other monomer, and subunit 6 with both core proteins of the other monomer. The dimer interface with the largest area is between cytochrome ***b*** in each monomer, chains C and P.

The "Core" Proteins Are Peripheral

The two largest subunits were labeled core proteins in 1967 (109) on the erroneous assumption that they form the core of the complex. They have sequence homology with a family of heterodimeric zinc proteases (103, 110) including insulinase and the general mitochondrial processing peptidase (MPP; EC 3.4.99.41). In fact, in some mitochondria the $\boldsymbol{bc_1}$ core subunits serve as the matrix processing peptidase (110–113). Surprisingly, the vertebrate and plant subunits 1 and 2 are more similar to the yeast MPP than to the yeast $\boldsymbol{bc_1}$ complex subunits. The function of these so-called core subunits in the $\boldsymbol{bc_1}$ complex, in relation to their homology and even processing peptidase activities, is an interesting story that will not be reviewed in depth here. (For more information see 110–113.)

Plant and trypanosome $\boldsymbol{bc_1}$ complexes tend to have three or more bands in the "core protein" region on SDS gels. This has been seen in wheat (Figure 6 in 114; 115), potato, yam, and beet (41), spinach (116), *Crithidia* (117), and *Trypanosoma* and *Leishmania* (EA Berry, LS Huang, A Horvath & D Maslov, unpublished results). Berry et al (41) suggested this may be a result of heterogeneity in one of the two subunits, as careful heme and protein analysis of the potato complex showed insufficient protein for three of these large subunits per cytochrome $\boldsymbol{c_1}$. Braun and coworkers (105) concluded that there were only two subunits in this molecular weight range, which they named α-MPP and β-MPP by sequence homology with the α- and β-subunits of the soluble MPP of rat liver mitochondria. The largest, β-MPP, has two isoforms, βI-MPP and βII-MPP. Although nearly identical in molecular weight, the isoforms are readily separated on Laemli glycine gels, giving the appearance of an extra core protein. They elegantly demonstrated this heterogeneity by using an antibody against βI-MPP to immunoprecipitate and enrich in dimers lacking βII-MPP (105).

The structure of the core proteins was described by Xia et al (14) from the tetragonal beef crystals, in which the core proteins were particularly well defined. As had been expected from sequence, similarity in the folds of the two subunits is high. An extensive dimer interface involves subunits 2, so they can be thought of as a dimer of heterodimers, which is attached to the dimeric $\boldsymbol{bc_1}$ subcomplex. Subunit 1 interfaces directly with cytochrome $\boldsymbol{b}$ in the same monomer, and the matrix-side ends of the transmembrane helices of the ISP, cytochrome $\boldsymbol{c_1}$, subunit 7, and subunit 10 are anchored in it. Subunit 2 contacts its symmetry-mate in the other monomer and subunit A; otherwise it is connected to the complex only by subunit 6 in the other monomer, which in turn contacts cytochrome $\boldsymbol{b}$. Subunit 9 is enclosed within subunits 1 and 2.

Predictions of the Fold and Heme Ligation of Cytochrome *b* Preceded the X-Ray Structures

The next three subunits in order of decreasing size are the three subunits with redox centers: cytochrome $\boldsymbol{b}$, cytochrome $\boldsymbol{c_1}$, and the Rieske iron-sulfur protein.

TABLE 7 Intersubunit contacts in the dimeric cytochrome bc_1 complex[1]

Chain Subunit	A (Core 1)	B (Core 2)	C (Cyt b)	D (Cyt c)	E (ISP)	F (SU 6)	G (SU 7)	H (Hinge)	I (SU 9)	J (SU 10)	K (SU 11)
A	•										
B	3998	•									
C	888		•								
D	339		3196	•							
E	2057		1061	1553	•						
F			2401	775		•					
G	1749		1931	1604	1124	997	•				
H				2272			385	•			
I	1084	3007							•		
J	345			1810	1286					•	
K	413				108					787	•

Chain **Subunit**	**A** **(Core 1)**	**B** **(Core 2)**	**C** **(Cyt b)**	**D** **(Cyt c)**	**E** **(ISP)**	**F** **(SU 6)**	**G** **(SU 7)**	**H** **(Hinge)**	**I** **(SU 9)**	**J** **(SU 10)**	**K** **(SU 11)**
N						191					
O		**1503**				835					
P			**2273**		1057						
Q				**553**[2]	709						
R			1047	709							
S	190	849									
T											
U											
V											
W											
X											

[1] Calculated from the structure 1BE3 after generating chains N-X from chains A-K by the appropriate symmetry operation.

[2] The interaction between cytochrome c_1 in the two monomers was taken from structure 1BCC, as 1BE3 shows no contact between these subunits. "Contact" was taken to mean approach of two atoms within 4 Å, center to center. Surface areas were measured using the CCP4 program AREAIMOL with a test sphere of the default radius, 1.4 Å.

Values in the cells are the amount of surface area buried by the interaction of the subunits whose chain letters are given at the top and right of the table. The chain letters A-K belong to one monomer, and N-X to the other. Thus the 10 contacts in the lower half of the table constitute the dimer interface. The three values in boldface indicate dimeric contacts between the same subunit in the two monomers. A hypertext version of this Table is available in the Supplemental Materials Section of the Annual Reviews site www.AnnualReviews.org, in which clicking on a subunit interface value takes the reader to a list of the specific atoms involved in the contact.

Cytochrome ***b*** behaves anomalously on SDS gels, running as a protein of much smaller molecular mass at low gel concentrations but approaching the mobility expected for its mass at high gel concentrations (118). In the range of 10%–12% polyacrylamide, the mobility is similar to that of cytochrome $\boldsymbol{c_1}$, and the two are often not resolved. In addition, the protein aggregates if boiled in SDS (118), and remains at the top of the stacking gel or at the interface between stacking and separating gels.

Early spectral kinetic studies showed at least two independent species, with three peaks in the α-band region (119). Potentiometric titrations of mitochondrial membranes show two and often three midpoint potentials attributable to ***b*** cytochromes (120). The two major components were designated cytochromes b_H and b_L, H indicating the higher and L the lower midpoint potential species. Cytochrome ***b*** can be purified from the complex, and in at least one preparation (121) the distinct potentiometric midpoints of the cytochromes are retained; however, the spectral differences are lost. There was considerable confusion about cytochrome ***b*** around the time of the Wainio monograph (3) and the Wikstrom (122) and Weiss (123) reviews on cytochrome ***b***. It was not generally accepted that the cytochrome ***b*** that Hatefi and coworkers (124, 125) correctly attributed to complex II really belonged to that complex rather than being a contaminant from complex III (122). The heme content of the Goldberger (126) preparation was one heme per 28 kDa of protein, in good agreement with the erroneous mass of around 30 kDa from sodium dodecyl sulfate–polyacrylamide gel electrophoresis (SDS-PAGE). The Ohnishi preparation (127) containing one heme per 21.3 kDa was inconsistent with this picture, but the preparation involved a proteolysis step. The real dilemma came in trying to explain the two or three species resolved in spectral, kinetic, or potentiometric experiments given only one chemical species. Weiss (123), among others, suggested that there were two identical cytochrome ***b*** subunits per cytochrome $\boldsymbol{c_1}$, but they interacted with different polypeptides in the complex, resulting in their different properties.

The key that solved the problem was the amino acid sequence of cytochrome ***b***, obtained from sequencing the mitochondrial genome (128, 129). This showed that the true molecular mass of the cytochrome ***b*** apoprotein was around 42.5 kDa, which together with the measured heme:protein ratio implied there must be two hemes per monomer. The two hemes would have different environments within the protein and thus different properties, accounting for the two species b_H and b_L. (The origin of the third, 150 mV component, will be considered later). Hydropathy plots predicted eight or nine transmembrane helices. As more sequences became available, the list of possible conserved heme ligands was narrowed down, and a nine-helix model for the folding and heme ligation of cytochrome ***b*** emerged (130, 131). Transmembrane helices 2 and 5, each with two histidines at the same level, one near the top and one near the bottom, were cross-linked by the hemes. This put the plane of the hemes parallel to each other, and perpendicular to the plane of the membrane (Figure 2), in agreement with EPR studies on oriented bilayers containing the $\boldsymbol{bc_1}$ complex (132).

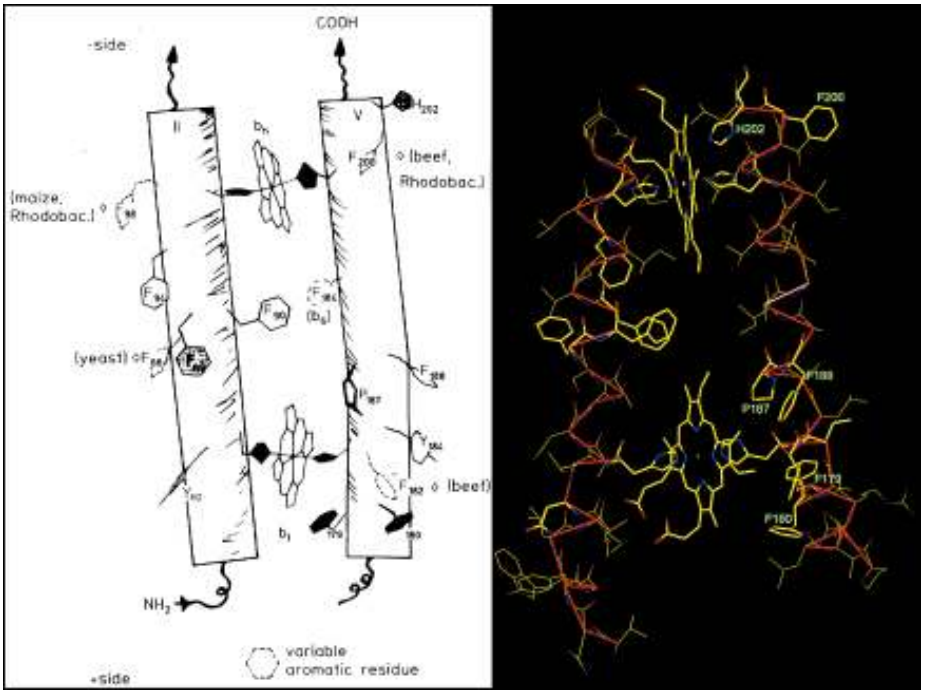

Figure 2 Ligation of cytochrome ***b*** hemes by histidines in two transmembrane helices. (*Left*) As envisioned based on hydropathy plots, natural sequence variation, inhibitor-resistant mutants, and site-directed mutagenesis. (*Right*) As determined by X-ray crystallography. [From Reference 132a (*left*) and from coordinates 1BCC (*right*).]

Further confusion arose from trying to fit the complicated phenomenology of cytochrome ***b*** oxidation-reduction with a linear electron flow scheme. This was cleared up by improved models leading to the modified Q-cycle, which will be discussed in a later section. The Q-cycle mechanism required two binding sites for quinone and specific inhibitors, and predicted which inhibitors should bind at each site. Mutations conferring inhibitor resistance in yeast were selected for and analyzed (133, 134). Using the model of nine transmembrane helices, residues conferring resistance to each inhibitor were found near both sides of the membrane, and so could not be arranged in clusters around single binding sites for each inhibitor. Helix 4 was weakly predicted, however, and by assuming that it was not transmembranous at all, a model was obtained in which the polarity of the remaining helices was flipped. This brought the resistance sites for inhibitors of the Q_i site to one side of the membrane and those for the Q_o site to the other side (135). This model with eight transmembrane helices turned out to be correct, and the weakly predicted transmembrane helix 4 (residues 139–167) forms two surface helices, now called cd1 and cd2, bent into a hairpin at the conserved P155.

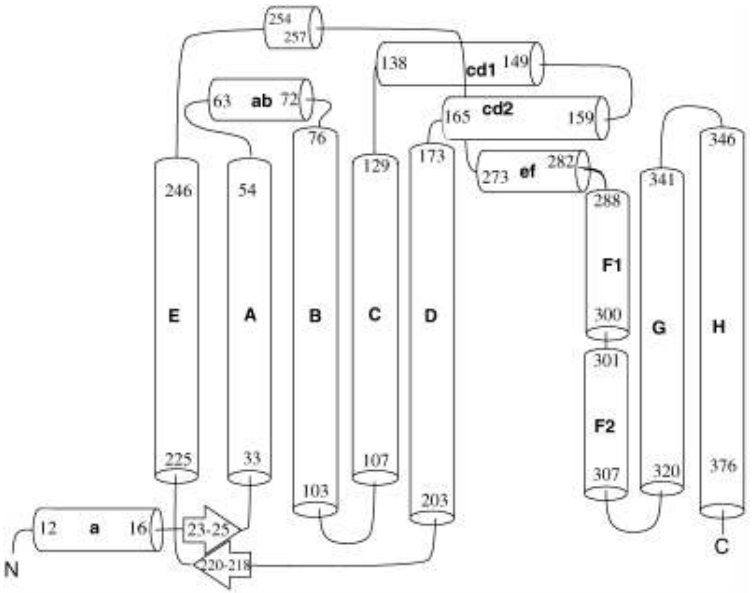

Figure 3 Secondary structure diagram of cytochrome ***b*** from structure 1BCC.

A tremendous number of cytochrome ***b*** sequences became available, largely as a result of the work of molecular evolutionists taking advantage of the simple maternal inheritance and lack of recombination of mitochondrial DNA. Site-directed mutagenesis defined the ligands for b_H and b_L (136). As the number of sequences grew, the number of totally conserved residues dwindled, and speculation on the function of highly conserved residues as well as clustering the natural inhibitor resistance and characterizing site-directed mutants led to further refinements in the model (137–140). It was recommended (137) that the eight transmembrane helices be designated with capital letters A–H, and the linker regions with lowercase ab, bc, cd, etc (see Figure 3). Conserved glycines in helices A and C were postulated to make room for close contact with the two hemes enclosed in a four-helix bundle consisting of helices A–D. The models arrived at (e.g. 137, 138) were remarkably accurate in their prediction of the relative positions of the eight transmembrane helices.

Cytochrome ***b*** is the only mitochondrially encoded protein in the $\boldsymbol{bc_1}$ complex. Experiments to engineer cytoplasmically synthesized constructs of cytochrome ***b*** for mitochondrial targeting in yeast were successful only for constructs containing three or fewer transmembrane helices (141).

In the X-ray structures, the four-helix bundle containing the hemes is twisted in a left-hand sense, resulting in a 45° angle between the planes of the hemes. The iron-to-iron distance between the high-potential and low-potential hemes is 20.7 Å (1BCC) and the closest approach of heme atoms is 7.9 between vinyl groups on

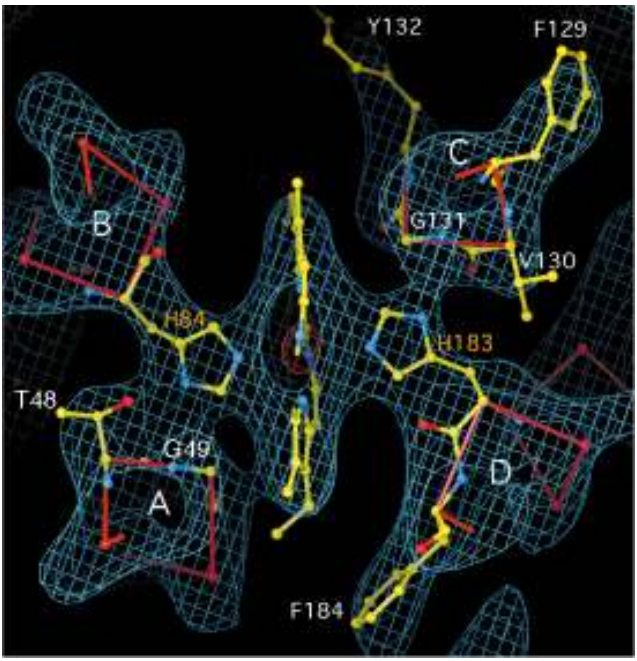

Figure 4 Electron density of heme-containing four-helix bundle, showing support of the axial-ligand imidazoles by all four helices. The structure is that of 1BCC, and the electron density map is calculated with experimental phases improved by averaging and contoured at 2.0 σ (*blue*) and 12.5 σ (*orange*).

the B pyrrole rings. Surprisingly, the low-potential hemes in the two monomers are quite close—21.2 Å between irons and 10.1 Å between vinyls on the C pyrrole rings. Possible implications for intermonomer electron transfer will be discussed later.

Figure 4 shows electron density superimposed on the model for the four-helix bundle and the low-potential heme. The heme plane lies between the A and B helices on one side and the C and D helixes on the other. The histidine heme ligands are shown. Although they arise from helices B and D, the liganding histidines are connected by density to both helices A and B (H84) and helices C and D (H183). H84 is covalently connected to helix B and H-bonded by Nδ to T48 on helix A, so that both helices support the imidazole in a position to bind the heme iron by Nε. Likewise, H183 in helix D H-bonds via Nδ to backbone atoms of helix C, so both helices support this imidazole. Cytochrome ***b*** contains the quinone and inhibitor binding sites Q_i and Q_o (or QN and QP) required by the Q-cycle mechanism, discussed later. Their structure will be described together with the discussion of mechanism.

The high-potential heme is close to the matrix surface of the cytochrome ***b*** subunit, and this surface is exposed to the aqueous phase in a cavity between the

core protein subunits. This is consistent with observations that this heme reacts with small water-soluble redox reagents (142), but not with estimates of the heme positions based on the relative magnitudes of the different phases of the flash-induced electrochromic band shift and a uniform membrane dielectric (143), or with interaction with soluble spin-relaxing reagents (144, 145). The low-potential heme is close to the exterior surface of cytochrome ***b***, but shielded from the aqueous phase by cytochrome $\boldsymbol{c_1}$.

Cytochrome c_1 Is a Class I Cytochrome

Cytochrome $\boldsymbol{c_1}$ was discovered in 1940 by Yakushiji & Okunuki (146) and independently by Keilin & Hartree (147). It was the second mitochondrial protein (cytochrome ***c*** was the first) to have its sequence determined (148). Yu et al (149) developed a purification procedure resulting in a subcomplex of cytochrome $\boldsymbol{c_1}$ with subunit 8. A preparation reportedly giving a single band was described by Konig et al (150). Kim & King (151, 152) later developed improved preparations of one- and two-subunit cytochrome $\boldsymbol{c_1}$. Subunit 8 [the "hinge protein for interaction of cytochrome $\boldsymbol{c_1}$ and cytochrome ***c***"(51)] was shown to be required for high-affinity binding of cytochrome ***c*** (151–153).

The bovine cytochrome consists of 241 residues, with a hydrophobic section near the C terminus (residues 204–222). Cytochrome $\boldsymbol{c_1}$ can be identified on gels by the color of the covalently bound heme in overloaded samples, or by fluorescence or peroxidase activity of the porphyrin or heme. Cloning and sequencing genes from various organisms showed that it is synthesized as a precursor with a leader sequence of about 80 residues (154). Li et al (155) purified the extrinsic domain of the *Neurospora* cytochrome $\boldsymbol{c_1}$ after proteolytic cleavage of the C-terminal membrane anchor.

The X-ray structure showed that the basic fold of cytochrome $\boldsymbol{c_1}$ is similar to that of cytochrome ***c*** and other class I cytochromes (15). It differs in having insertions and deletions in the various linker peptides between the core helices. Cytochrome $\boldsymbol{c_1}$ has a long N-terminal extension before the first helix, which interacts with the hinge protein (subunit 8). There is a long bifurcated loop (Y-loop) between the heme-binding CXXCH sequence and the heme-bracing PDL sequence, which seems to be involved in cytochrome ***c*** binding and in dimerization of the $\boldsymbol{bc_1}$ complex. The linker between the –PDL– sequence and helix 3, which is long and covers the heme propionate edge in cytochrome ***c***, is greatly shortened in cytochrome $\boldsymbol{c_1}$ and leaves this edge of the heme exposed for electron transfer from the Rieske protein (Figure 5). The loop between the axial-ligand methionine and helix 5 is longer in cytochrome $\boldsymbol{c_1}$ and is probably involved in cytochrome ***c*** binding.

Cytochrome $\boldsymbol{c_1}$ is the only one of the seven transmembrane subunits that does not have its N terminus on the matrix (N) side of the membrane. In the Schagger fractionation of the bovine complex by detergent and chaotropes (27), cytochrome $\boldsymbol{c_1}$ was initially obtained together with subunits 8 and 10, and in a subsequent step the two small subunits were removed using higher concentrations of guanidinium.

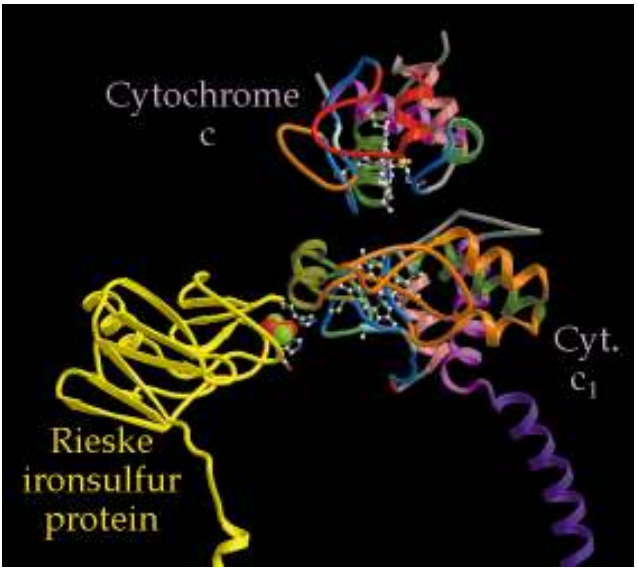

Figure 5 Model of the high-potential electron transfer chain of the $\boldsymbol{bc_1}$ complex. The Rieske ISP and cytochrome $\boldsymbol{c_1}$ are from our beef P6522 crystals. Cytochrome $\boldsymbol{c}$ is positioned to appose the exposed C corner of the cytochromes $\boldsymbol{c}$ and $\boldsymbol{c_1}$. *Red* and *green spheres* represent the $[Fe_2S_2]$ cluster, and *gray ball-and-stick models* represent the hemes. (From Reference 15.)

In the X-ray structure, subunit 8 is bound to the side of the extrinsic domain of cytochrome $\boldsymbol{c_1}$, contacting mainly the N-terminal extension. Subunit 10 contacts cytochrome $\boldsymbol{c_1}$ along the transmembrane helix near the P side (residues 199–211), in the N-terminal extension (residues 13–27), and in the first branch of the Y-loop (residues 53–60). Residues near the C terminus of cytochrome $\boldsymbol{c_1}$ (234–238) and the N terminus of subunit 7 (10–14) contribute two more beta-strands to a 6-stranded beta sheet of subunit 1, designated sheet B of chain A in the entry 1BCC. The N-terminal residues of the ISP also pass near here, but are not part of the beta-sheet in the structures published to date.

The measured angle of the heme plane to the membrane plane is 72°, fairly consistent with the EPR results indicating nearly perpendicular planes (132). However, a recent linear dichroism study indicates a smaller angle of 57° (156). The authors suggested the possibility of movement of cytochrome $\boldsymbol{c_1}$ under the conditions of the experiment.

The Rieske Iron-Sulfur Protein Has a Mobile Redox Center

The presence of an iron-sulfur cluster in the $\boldsymbol{bc_1}$ complex was recognized by its contribution to the EPR spectrum (19). Originally noted as the $g = 1.9$ iron-protein, the Rieske iron-sulfur protein, as it is now called, was isolated in a succinilated

form from a residue of insoluble protein split off the antimycin-treated complex III by taurocholate and $(NH_4)_2SO_4$ (157).

The Racker lab split the succinate:cytochrome c reductase (SCR) complex with bile salts in the absence of antimycin into a soluble fraction containing cyt $\boldsymbol{c_1}$ and an insoluble fraction containing cytochrome ***b***, which could be combined to generate antimycin-sensitive succinate:cytochrome ***c*** reductase. Further resolution of the soluble fraction revealed an essential component other than cytochrome $\boldsymbol{c_1}$, which was named oxidation factor (158). Trumpower & Edwards (6) purified this oxidation factor and showed it to be a reconstitutively active form of the Rieske iron-sulfur protein. The von Jagow group used the nonionic detergent Triton X-100 to resolve and reconstitute the mitochondrial Rieske protein (159).

In classical ferredoxin-type [2Fe-2S] centers, the ligands are all cysteine residues (via the γ-sulfur), and alignments of Rieske ISP proteins show four conserved cysteines as potential ligands. However, Electron Nuclear Double Resonance [ENDOR (160)] and Electron Spin Echo Envelope Modulation [ESEEM (161)] spectroscopy indicated that two of the ligands were nitrogenous and probably histidine. The roles of the four conserved cysteines and two conserved histidines have been tested by site-directed mutagenesis (162, 189), and all were found to be essential. Davidson et al (162) found a small amount of atypical EPR signal in the Rieske region in the C155 mutant (corresponding to C160 in beef). Alignment with bacterial aromatic dioxygenases, which have similar N,S ligation of the cluster, showed that C138 and C155 (corresponding to bovine C144 and C160) were not conserved. They speculated that these two residues were not ligands but formed a disulfide that is important for the stability of the cluster. This has been confirmed by the X-ray structures.

The ISP [2Fe-2S] cluster in the reduced form is paramagnetic with a characteristic $g = 1.9$ EPR signal, the g_x band of which is sensitive to the occupant of the Q_o site (85). The g_x band is broad with a peak at 1.75–1.77 in the isolated Rieske fragment, or in the complex in situ if the Q_o site is empty or contains reduced ubiquinol or an MOA inhibitor. Quinones or the inhibitors UHDBT and stigmatellin enhance the g_x peak and shift it upfield, giving peaks at 1.80 or 1.79, respectively (85, 163–165, 252).

The mature iron-sulfur protein has 196 residues (beef) with a membrane anchor of one transmembrane helix near the N terminus. It is translated with a leader peptide of 78 residues (beef) or 30 residues (yeast). All the residue numbers used below refer to the mature protein rather than the precursor.

Li and coworkers (166) prepared a soluble form of the ISP from *Neurospora* by limited proteolysis. Gonzalez-Halphen et al (287) prepared such a construct from the bovine Rieske protein by trypsinization. Link et al (73) used thermolysin to cleave the bovine Rieske protein before residue 68. The water-soluble product was extensively characterized and was crystallized, and the X-ray structure by Iwata et al (74) provided the first atomic-resolution structure of a part of the mitochondrial $\boldsymbol{bc_1}$ complex.

Mutation of residues involved in hydrogen bonds to the iron-sulfur cluster result in reducing the redox midpoint potential of the cluster and decreasing the

steady-state turnover of the enzyme in yeast (167), *Paracoccus* (168), or *Rb. sphaeroides* (169–170a). The good correlation between midpoint potential of the ISP (or equivalently ΔG for its reduction) and the steady-state turnover rate indicate that reduction of the ISP is at or before the rate-limiting step in the enzymatic mechanism (see below).

The transmembrane region of the $\boldsymbol{bc_1}$ complex dimer consists of two bundles of symmetry-related transmembrane helices, and the helices making up each bundle have been assigned to one monomer (division of a dimer of multiprotein complexes into monomers is in principle arbitrary, but it makes sense to choose monomers so that the elements are in contact). This assigns the ISP to the monomer with which its transmembrane helix is associated. However, the extrinsic domain crosses over and associates with cytochromes $\boldsymbol{b}$ and $\boldsymbol{c_1}$ of the other monomer. Thus dimerization is required to complete the high-potential chain. It is unlikely that the extrinsic domain of the ISP could twist around and react with cytochrome $\boldsymbol{b}$ of its own monomer. This is important with reference to reports of active monomers of the complex (28, 171); however, it is possible that conditions leading to monomerization would also lead to loosening (though not complete release) of the ISP from the complex, so that it would be able to react within a monomer.

The extrinsic domain of the ISP was not well ordered in the first X-ray structure of the mitochondrial $\boldsymbol{bc_1}$ complex (14), structure 1QCR; but the iron-sulfur cluster could be located by anomalous diffraction of its iron atoms. The cluster was close to the surface of cytochrome $\boldsymbol{b}$, the so-called proximal or $\boldsymbol{b}$ position. The order was somewhat better in the chicken structure (15), structure 1BCC; and the high-resolution structure of the soluble fragment from Iwata et al (74), structure 1RIE, could be positioned in the density without ambiguity. The position of the cluster was quite different from that in the tetragonal beef crystals, however, being closer to the heme of cytochrome $\boldsymbol{c_1}$ and farther from cytochrome $\boldsymbol{b}$, the distal or $\boldsymbol{c_1}$ position. If the complex was treated before crystallization with stigmatellin, which is known to bind in a site involving both the ISP and cytochrome $\boldsymbol{b}$ (85), then the cluster was found in the cytochrome $\boldsymbol{b}$ position as in the 1QCR structure. This, together with the poor order of the ISP in the 1QCR structure, suggested that mobility of the ISP was important to the function of the complex (15, 84). The movement of the extrinsic domain of the ISP and its implications for the mechanism will be taken up again in a later section.

Refinement of the ISP structure by Iwata et al (16) in the hexagonal bovine crystals suggests an internal conformational change. In the $P6_522$ crystals (1BE3) the conformation is the same as in the structure of the soluble fragment 1RIE. In the $P6_5$ crystal (3BGY) the asymmetric unit contains a dimer, so there are two copies of the ISP, assigned chain letters E and Q. The Q chain is complete, and in this model there is an internal conformational change in which the cluster-bearing loops rotate slightly relative to the basal fold, and P175 goes from the *trans* to *cis* conformation. Analysis of a dataset from the tetragonal crystals of the type prepared by Yu and coworkers with the Rieske protein in the cytochrome $\boldsymbol{b}$ position suggests that here also the ISP has the altered internal conformation with the *cis* form of P175 (S Iwata, personal communication).

Small Subunits of the bc_1 Complex

Subunits 6 and 7 have both been called quinone binding proteins, but from the structure it appears that neither has any role in either of the known quinone binding sites. The relative mobility on SDS gels depends on the system used, so that in the Weber and Osborne phosphate gels used in the original studies, subunit 6 becomes subunit 7 and vice versa.

Yu and coworkers (172–173) identified two subunits labeled by quinone-analog photoaffinity labeling. One was subunit 3 (cytochrome ***b***) and the other was a small subunit, subunit 6 in their gels but equivalent to subunit 7 of the Schagger Tricine gels. It was soon isolated and sequenced (174). Later the photoaffinity-labeled subunit 7 was isolated and the label was localized to a peptide comprising residues 48–57 (175). This is within the transmembrane helix, near the center of the membrane, but not near either quinone binding site.

Wang & King (176) named subunit 7 of the phosphate gels (subunit 6) QPc based on reconstitution of quinol:cytochrome ***c*** reductase activity to a preparation considered depleted of quinone binding protein. This protein was sequenced in 1985 by Wakabayashi et al (177) under the name QPc. By this time the gene for the 14-kDa subunit of the yeast $\boldsymbol{bc_1}$ complex had been sequenced (178), and comparison of the new sequence showed it to be homologous. The yeast subunit 6 precursor has an atypical 25-residue presequence. However, this is not required for mitochondrial import, rather the C-terminal section may be implicated as important for import (179).

From the X-ray structures, subunit 7 has a single hydrophobic transmembrane helix. This is consistent with the fact that it is labeled by the hydrophobic quinone analogs. Subunit 6 is a relatively hydrophilic protein, sandwiched between subunit 2 and cytochrome ***b***. At first glance it seems unlikely that it could be removed and added back to the complex, but in fact it is located in shallow notches on the sides of the dimer at the junction between the core proteins and cytochrome ***b*** (see the left-hand dimer in Figure 1). If the resolution and reconstitution experiments of Wang & King can be repeated they might provide valuable information about the function of this supernumerary subunit.

Subunit 9 of the bovine complex is the presequence of the ISP and has no homolog in the yeast or potato complexes. Sequence was assigned in 1QCR and in the structures from Uppsala (1BE3 and 3BGY); however, the assignments are not consistent, even with respect to sequence direction: residues 21–43 of 1QCR correspond to residues 60–46 of 1BE3. Sequence was not assigned for this subunit in the chicken structures, but chain I was used to trace several unassigned densities in the core region with polyalanine. It turns out that residues 105–118 of this polyalanine correspond to residues 65–78, the β-hairpin at the C terminus in 1BE3. These two strands make a β sheet with residues 96–100 of subunit 2 in that structure. Residues 202–208 of the chicken structure are close to residues 38–43 of 1QCR; the Uppsala structures have nothing here.

Subunits 10 and 11 are small hydrophobic proteins making a single transmembrane helix each. Subunit 11 is the first protein to be dissociated if the complex is delipidated by binding to hydroxyapatite and washing with increasing Triton X-100 concentrations (180). Full activity can be restored to the subunit-11–depleted complex by adding only phospholipids, so subunit 11 is not required for activity (180). When the beef bc_1 complex is fractionated according to Schagger et al (27), the first two subunits to be removed are subunit 11 and the Rieske protein; and subunit 11 has become known as the Rieske associated protein. No density was found for subunit 11 in the orthorhombic chicken bc_1 crystals, although it was seen by the same authors in the lower resolution hexagonal and monoclinic beef crystals. Subunit 11 also was not detected by SDS-PAGE in the chicken bc_1 preparations used for crystallization (15), although mass spectroscopy detected a fragment about the right size (6315–6419 Da) in some preparations (S Yoshikawa, personal communication). It seems likely that this subunit is present in the chicken complex, but that it is removed by detergents even more readily than the beef subunit is. Thus it is lost to a variable extent during purification, and even more may be lost upon addition of additional detergent for crystallization.

Subunit 10 is seen in all the structures, and they all superimpose well from the N terminus to residue 45. After that the protein in 1QCR diverges sharply from that in 1BCC and 1BE3, which agree well except the last two residues. Residues 48–61 of subunit 10 in 1QCR superimpose with residues 1–15 of cytochrome c_1 in 1BCC or 1BE3, but with the direction reversed. Subunit 11 is present in all the beef structures. Superposition is good between 1QCR and 1BE3 over the range where both were built (1QCR includes the entire N terminus and more on the C terminus than 1BE3).

SUBUNITS OF THE b_6f COMPLEX

The b_6f complex prepared by Hurt & Hauska (45) had five bands on SDS gels. The two largest bands corresponded to two forms of cytochrome *f*, and the next two were cytochrome *b* and the Rieske ISP (181). The fifth band, or the fourth distinct polypeptide, was subunit IV, later shown to have sequence homology with the C-terminal part of cytochrome *b* (131). In addition to the five bands originally noted, the preparation contained several low-molecular-weight bands (181). There are at least three small subunits in higher plant b_6f; the three that have been sequenced are called PetA, PetM, and PetL (=ycf7) (182–185). Cytochrome *b* and *f* are both encoded on plastid genes. The ISP and small Pet subunits are nuclear.

The b_6f complex as isolated contains chlorophyll and carotenoid. Attempts to remove these "contaminants" led to the conclusion that there is one mole each of specifically bound chlorophyll *a* and carotenoid (63, 186, 187) associated with the complex. The carotenoid has been suggested to protect against free radicals formed at the Q_o site (188).

Cytochrome b_6 and Subunit IV

Cytochrome $\boldsymbol{b_6}$ has good homology with the region of cytochrome ***b*** including helices A–D. Residues in the vicinity of the Q_o site are well conserved between mitochondrial cytochrome ***b*** and cytochrome $\boldsymbol{b_6}$. In subunit IV, the PEWY sequence, of which E272 is probably a ligand for ubiquinol, is conserved. At the Q_i site, the quinone-ligand H202 is replaced by R, and D229 by E.

The heme is often detected in the cytochrome $\boldsymbol{b_6}$ band after SDS gel electrophoresis (e.g. 181). Several treatments aimed at removing noncovalently bound heme, including extraction with phosphate/acetone, acid/acetone, plus heating at 100°C for 50 s in the presence of 2% SDS, were unsuccessful in completely extracting the heme from cyt $\boldsymbol{b_6}$ of *Chlamydomonas reinhardtii* (190). This led to the suggestion that at least one of the two hemes (most probably heme b_L) may be covalently bound in the $\boldsymbol{b_6f}$ complex of this alga (190). Mutagenesis studies in *Bacillus subtilis* suggested that it is the high-potential heme that is covalently bound, and a conserved cysteine (C35 in spinach cytochrome $\boldsymbol{b_6}$) near the start of helix 1 has been proposed (191) to provide a thioether linkage as in ***c*** cytochromes. However, cytochrome $\boldsymbol{b_6}$ from spinach is not heme-stainable if the sample is heated moderately with urea before electrophoresis (G Hauska, personal communication), so it seems more likely that heme is retained as a result of incomplete unfolding of cytochrome $\boldsymbol{b_6}$ in SDS under the usual conditions. The residues corresponding to this cysteine in chicken and beef cytochrome ***b*** are N33 and N32, and both of these face away from the heme. Since G37 (spinach) is conserved in both cytochrome ***b*** and $\boldsymbol{b_6}$ and is required for a heme contact, it is likely that the orientation of this part of the helix relative to the heme is the same in cytochrome ***b*** and $\boldsymbol{b_6}$, in which case C35 is on the wrong side of the helix to covalently bind the heme.

The b_6f Rieske ISP

Malkin et al (192) purified the chloroplast Rieske protein from thylakoid membranes. It was later purified from the isolated $\boldsymbol{b_6f}$ complex (193). The ISP seems to be even more readily dissociated from the complex than in the mitochondrial case. Szczepaniak et al (194) found that cytochrome ***b***, subunit 4, and the Rieske protein were extracted from thylakoid membranes, in that order, by alkaline wash. Breyton et al (195) agreed that the chloroplast ISP is resistant to alkaline or salt extraction, but found it is rather easily extracted by chaotropes, and suggested that it may be an extrinsic protein.

There is spectroscopic (68) and electron microscopic (67) evidence for movement of the chloroplast Rieske induced by inhibitors, making it likely that movement of the ISP is also part of the catalytic cycle in this complex. In fact, since the structure of the chloroplast ISP and the sequence of cytochrome $\boldsymbol{b_6}$ + subunit IV are so similar to the mitochondrial counterparts, it can be expected that if the ISP were in position to react with the Q_o site, its cluster would be shielded from cytochrome ***f*** by the cytochrome ***b*** protein, and so some motion would be necessary.

Cytochrome *f*

The orientation of the heme of cytochrome ***f*** to the plane of the bilayer membrane has been estimated by EPR spectroscopy of oriented multilayers (196–198). Unlike cytochrome $\boldsymbol{c_1}$, which has the heme nearly perpendicular to the membrane (132) or 73° in the structure 1BCC, the cytochrome ***f*** heme plane makes an angle of 25–30° with the membrane. Linear dichroism experiments (199) indicate an angle of 50–54°.

The extrinsic domain of cytochrome ***f*** is elongated with a large and small domain (69). The heme is in the large domain, near the interdomain interface. The N-terminal residue is in the large domain and its amino nitrogen serves as an axial ligand for the heme. The C terminus of the soluble construct, where the transmembrane helix begins, is in the large domain at the end opposite the interdomain interface. The heme propionates are exposed, and the vinyl group on pyrrole ring C is exposed through a deep well. In the chloroplast cyt ***f*** there is a cluster of basic residues at the domain interface that has been proposed to be involved in binding plastocyanin (69, 70, 200). The importance of these residues for plastocyanin binding depends on experimental conditions such as ionic strength (201, 202). The cyanobacterial cyt ***f*** (72) is less basic and has no basic patch, and cyanobacterial plastocyanin is correspondingly less acidic.

There is a solution structure for plastocyanin transiently bound to cytochrome ***f*** (203) at ionic strength well below physiological but high enough that complex formation is transient. This structure is based on a new approach using molecular dynamics and the known structures of cytochrome ***f*** and plastocyanin, with experimentally determined chemical shift changes and intermolecular pseudocontact shifts in the plastocyanin spectrum as restraints. This structure mates the basic patch with acidic residues on plastocyanin and puts the copper of plastocyanin close to the cytochrome ***f*** heme propionates and Y1, which stacks with the heme ring. Note that in the $\boldsymbol{bc_1}$ complex it is the Rieske protein that interacts with the propionate edge, and the electron acceptor is presumed to interact with the pyrrole C corner. Thus if both cytochromes have separate entry and exit ports for electrons, and the solution structure from nuclear magnetic resonance (NMR) actually represents the reaction complex, then the direction of electron throughput would seem to be reversed in cytochrome ***f***.

The long axis of the protein makes an angle of approximately 20° with the heme plane. In considering the constraints placed by the approximately 27° angle (between heme plane and the membrane) on the orientation of the protein, the cytochrome could be rotated freely about the heme normal without changing the angle of the heme plane to the membrane. At one extreme the angles would add, giving an angle of 20 + 27° between the long axis and the membrane plane, and at the other extreme they will subtract, giving 20 – 27°. Thus any angle of the long axis to the membrane plane between 0 and 50° could be consistent with the observed heme angle.

Cramer and coworkers (204) propose that the long axis is nearly parallel to the membrane. This together with the heme orientation of 25–30° leaves the heme

face and lysine cluster exposed for interaction with plastocyanin, puts the large and small domains of the cytochrome somewhat in the positions of cytochrome $\boldsymbol{c_1}$ and the hinge protein in the $\boldsymbol{bc_1}$ complex, and may provide a justification for a water chain to serve as a sort of proton wire through cytochrome ***f***.

On the other hand, two crystal forms of Kuras & Wollman's truncated *Chlamydomonas* cytochrome ***f*** (205), belonging to different space groups, both contain an intimately associated dimer related by a twofold noncrystallographic axis, suggestive of a physiological dimer (206) (Figure 6). This dimer leaves the plastocyanin binding site observed in the structure 2PCF exposed for reactions, along with the well leading to the vinyl on ring C of the heme. It puts the C termini, and thus the transmembrane helices, of the monomers about 90 Å apart. The two heme irons are 31 Å apart. If this is the physiological dimer and the twofold axis is perpendicular to the membrane, the hemes make an angle of 79° with the membrane, similar to the case in cytochrome $\boldsymbol{c_1}$ but inconsistent with either the EPR or linear dichroism studies on cytochrome $\boldsymbol{b_6f}$ mentioned above.

MECHANISTIC INVESTIGATIONS OF bc_1 COMPLEXES

The Modified Q-Cycle

In the following we assume that the $\boldsymbol{bc_1}$ complex operates through a modified Q-cycle mechanism (9, 12, 207–211), as summarized in Figure 7. We believe such a mechanism adequately accounts for most of the experimental results, and that results which appear contrary will be resolved by refinement of the mechanistic model or by better understanding of the experiments. Most investigators working in the field seem to share this feeling. However, this is not unanimous and we should point out that certain well-respected investigators (212–214) feel the Q-cycle mechanism is likely to be seriously in error.

Quinol is oxidized at the Q_o site of the complex in a reaction with a relatively high activation barrier (210). One electron is transferred to a high-potential chain and the other to a low-potential chain, in the so-called bifurcated reaction. The high-potential chain, consisting of the ISP, cyt $\boldsymbol{c_1}$, and cyt ***c*** (or $\boldsymbol{c_2}$), transfers the first electron from quinol to an acceptor (cytochrome oxidase in mitochondria, the oxidized photochemical reaction center in photosynthetic systems). Cyt ***c*** acts as a mobile species, reacting with cyt $\boldsymbol{c_1}$ through a binding site on the P-side surface. The low-potential chain consists of two cyt ***b*** hemes, which form a pathway through which electrons are transferred across the coupling membrane from the Q_o site to the Q_i site. Because QH_2 oxidation is the limiting step, and proceeds through a high activation barrier, the reaction at the Q_o site appears to be a concerted electron transfer to the high- and low-potential chains. It is generally supposed that an intermediate semiquinone is generated at the Q_o site, but this has not been detected (210, 215). In order to provide the two electrons at the Q_i site required for reduction of quinone, the Q_o site oxidizes two equivalents of quinol in successive

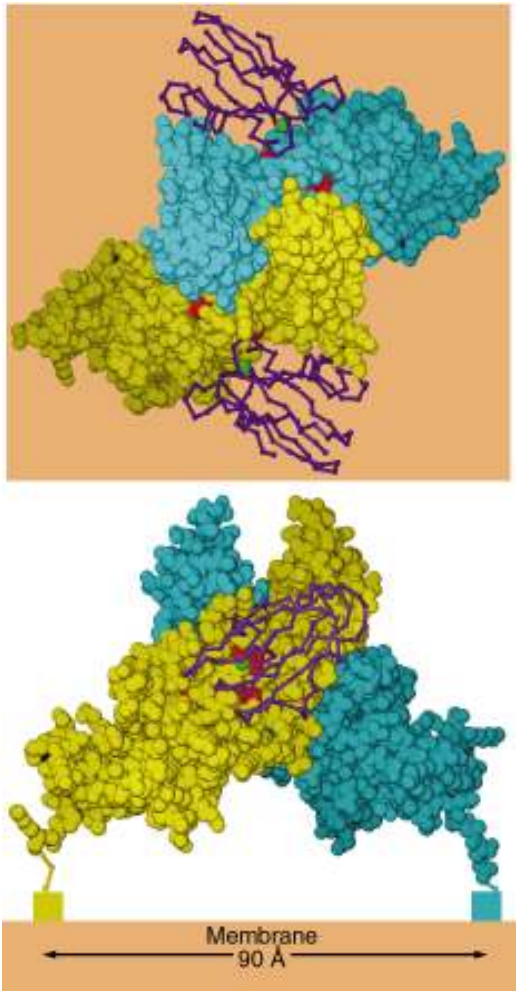

Figure 6 Dimeric cytochrome ***f*** found in two crystal forms of *Chlamydomonas* cytochrome ***f***. The *upper panel* shows a top view, looking down the twofold axis of symmetry. The *lower panel* is a side view looking parallel to a hypothetical membrane plane constructed perpendicular to the twofold. The *blue* and *yellow space-filling models* are monomers a and b (from two different asymmetric units) from the structure 1CFM. The hemes are shown as *red space-filling models*. The *magenta* backbone drawings are plastocyanin from structure 2PLT, oriented relative to the cytochrome ***f*** monomers as in the NMR structure of the complex between poplar plastocyanin and turnip cyt ***f*** (2PCF). The copper atom of plastocyanin is shown as a *green sphere*. (From Reference 206.)

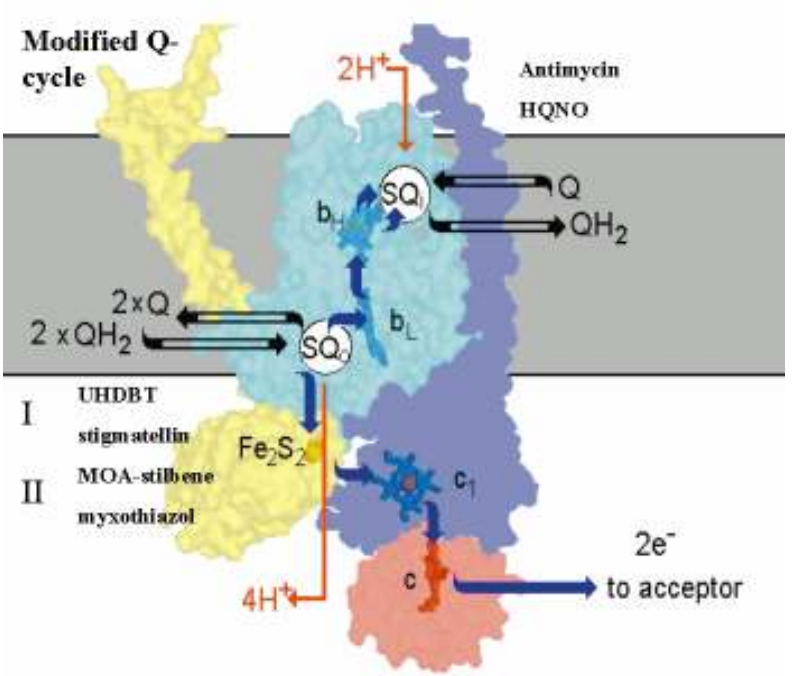

Figure 7 Schematic representation of the modified Q-cycle in the context of the structure. The structure of a "functional monomer" of the $\boldsymbol{bc_1}$ complex abstracted from structure 1BCC (15) is shown, with the catalytic sites emphasized. The binding of cyt ***c*** (*red*) to cyt $\boldsymbol{c_1}$ (*blue*) is shown by a model of yeast cyt ***c*** positioned as in Figure 6. The Q_o and Q_i sites in cyt ***b*** (*cyan*) are indicated by SQ_o and SQ_i for the intermediate semiquinone species thought to function at the sites. The ISP is shown in *yellow*. Protein is represented by the surfaces of the subunits; prosthetic groups are shown with metals indicated by *space-filling spheres,* and heme rings by *stick models,* labeled as follows: Fe_2S_2, [2Fe-2S]-cluster; c_1, heme c_1; b_L, heme b_L; b_H, heme b_H. Inhibitors discussed in the text are indicated close to the site at which they function. Electron transfer events are shown by *solid blue arrows,* proton uptake or release is indicated by *thin red arrows*; substrate and product binding by *open black arrows*. The coupling membrane is represented by the *gray area*.

turnovers (143, 216, 217). The first electron at the Q_i site generates a relatively stable semiquinone that is reduced to quinol by the second electron. The overall reaction generates four protons in the intermembrane space (or periplasmic space in bacteria), called the P-side for its positive protonic potential, and the formation of quinol uses up two protons from the mitochondrial matrix (or cytoplasmic side), called the N-side for its negative protonic potential,

$$QH_2 + 2\text{cyt}\ \boldsymbol{c}^{3+} + 2H_N^+ \Leftrightarrow Q + 2\text{cyt}\ \boldsymbol{c}^{2+} + 4H_P^+.$$

Mechanism of Quinol Oxidation at the Q_o Site of the Complex

The reaction at the Q_o site determines the unique functional characteristics of the $\boldsymbol{bc_1}$ complex. The bifurcation of the two electrons from quinol between high- and low-potential chains is crucial to the process through which the free-energy drop between the quinol pool and oxidized acceptor is used to generate a proton gradient. The efficiency of this process is a primary determinant in energy conversion, and any loss through decoupling would result in a competitive disadvantage. The complex has evolved to maximize the efficiency, and achieves a remarkable partitioning in which the second electron is passed almost exclusively to the low-potential acceptor provided by heme b_L, despite the availability of a thermodynamically much more favorable pathway to the high-potential chain.

Antimycin, by blocking the Q_i site, acts as an effective inhibitor of net electron transfer by the $\boldsymbol{bc_1}$ complex. Under steady-state conditions in the presence of antimycin, the low-potential chain becomes reduced, removing heme b_L as an acceptor of the second quinone. The high-potential chain remains oxidized, so that the Q_o site is poised with excess of substrate (quinol and ISP_{ox}) so as to strongly favor formation of the semiquinone product of the first electron transfer reaction. These conditions are referred to as oxidant-induced reduction, since they lead to reduction of cyt ***b*** on addition of an oxidized acceptor, but thereafter to an inhibited chain. Inhibition of the reaction is the paradox of the bifurcated reaction, since the high-potential chain is available to accept electrons, but no flux is observed. De Vries et al (218) showed that although no reduced ISP could be detected by EPR, a weak semiquinone signal that was insensitive to antimycin but sensitive to British Anti-Lewisite (BAL), was present in mitochondrial preparations. Andrews [211, quoted in Crofts & Wang (210)] could detect no myxothiazol-sensitive semiquinone under these conditions, and the authors therefore concluded that the equilibrium constant for formation of semiquinone was very small, and that $\Delta G^{o'}$ was large and positive, and might contribute a significant part of the activation barrier. This view has recently been reinforced by similar observations in mitochondrial preparations (215). Link (219) has suggested that a relatively stable complex of ISP_{red} with semiquinone might be formed, but that both EPR signals might be lost through interaction between their neighboring spins. In the presence of O_2, a weak antimycin-insensitive electron transfer is observed, and this has been attributed to reduction of O_2 to O_2^- by semiquinone or heme b_L (220, recently reviewed in 221). Similarly, under aerobic static-head conditions, electrons accumulate on heme b_L as a result of back-pressure from the proton gradient, but flux is minimal and mainly attributable to proton leakage or O_2^- formation rather than mechanistic decoupling. It is clear from the low leakage rate that if any semiquinone is formed, it is unable to reduce the high-potential chain rapidly.

The mechanism of the Q_o site reaction has been much studied, but details are still controversial. Following earlier Q-cycle models (9, 207, 208), Crofts & Wang (210) proposed a detailed mechanism that provided an excellent fit to the kinetics of flash-activated turnover of the $\boldsymbol{bc_1}$ complex in *Rb. sphaeroides* under a wide range

of conditions, and also accounted well for the kinetics of the mitochondrial complex. This modified Q-cycle model requires some revision to take account of the new structural information (14–16, 84, 222). In particular, the reaction schemes previously proposed for the Q_o site need to be extended to take account of the movement of the ISP. Since both quinol and the ISP head are mobile species, formation of the enzyme-substrate complex requires docking of both in an appropriate configuration (169, 223), as summarized in the scheme below.

$$E.c_1^{+}.H\text{-}ISP^{C}_{red} \leftrightarrows E.c_1 + H\text{-}ISP^{C}_{ox}$$

$$H\text{-}ISP^{C}_{ox} \leftrightarrows ISP^{C}_{ox} + H^{+}, \quad pK \sim 7.6$$

$$ISP^{C}_{ox} \leftrightarrows ISP^{B}_{ox}$$

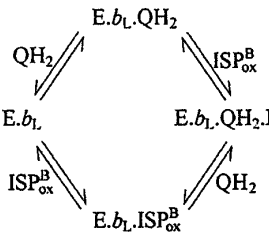

$$\leftrightarrows \{ES^{\#}\} \leftrightarrows [E.b_L.QH^{\bullet}.H\text{-}ISP^{B}_{red}] \leftrightarrows E.b_L^{-} + Q + H\text{-}ISP^{(free)}_{red},$$

where cyt ***b*** with heme b_L is represented by E.b_L, cyt $\boldsymbol{c}_1$ and its heme by E.c_1, the transition state by {$ES^{\#}$}, and the docking of the ISP is indicated by subscripts C and B to indicate enzyme-substrate complexes on cyt $\boldsymbol{c}_1$ and cyt ***b***, respectively. The movement of the ISP requires that five catalytic interfaces participate in turnover, rather than the three in earlier Q-cycle mechanisms.

The modifications above are demanded by the structure. Other aspects of the Crofts-Wang model have been challenged on other grounds.

1. Several different groups (165, 218, 224–229) have proposed that catalysis involves a synergistic interaction between two quinones occupying the site simultaneously (double-occupancy models), or interaction between monomers (230). The most compelling case for double-occupancy has been based on properties of the $g_x = 1.80$ and $g_x = 1.783$ EPR signals associated with interaction between quinone and the ISP_{red}, and the effects of extraction of the quinone pool. The two signals were attributed by Ding et al (165, 224) to two species, Q_{ow} (weakly binding) and Q_{os} (strongly binding) respectively, with >ten-fold differences in affinity for the Q_o site, and interpreted in terms of a double-occupancy mechanism in which the two species act synergistically, and occupy the site together.
2. It has been suggested that the activation barrier involves the deprotonation of quinol (226–229), or simultaneous electron transfer to both acceptors

(84), or that the rate-limiting step is the second electron transfer on oxidation of semiquinone, and that the latter is formed as a relatively stable intermediate in the transition complex (16, 219).

3. Several different mechanisms have been proposed to resolve the paradox of the bifurcated reaction (see above), which combine some of the modifications suggested in items 1 and 2 above with a variety of switching mechanisms controlled by later redox events (16, 84, 226–229).

These mechanisms are not necessarily mutually exclusive, but analysis in the light of the structures (14–16, 84, 222) might allow some critical distinctions.

Mutations Affecting Inhibitor Binding or Function at the Q Sites

Earlier work on mutations in the bc_1 complex has been admirably summarized by Brasseur et al (231). The predicted location of the quinone processing sites, based on these earlier studies and structural prediction (138–140), was confirmed by the structures (14–16, 222). Crofts, Berry, and colleagues (92–94, 169, 222) have made a more detailed analysis of the relation between functional effects and the location of these mutation sites in the structures. The distribution of sites affecting inhibitor binding was, with few exceptions, consistent with the binding domains of the inhibitors, since they impinged directly on the inhibitor binding interface. Most exceptions could be rationalized in terms of structural dislocation due to packing, H-bonding, etc, close to the sites affected. Of particular interest was the location of mutations that affect the $g_x = 1.80$ signal, observed when the quinone pool is oxidized and ISP reduced, and attributed to interaction of a weakly binding quinone with the ISP_{red} (165, 163). On the basis of correlation of these effects with function, three different sets of mutations were noted (222, 223, 232).

1. Changes around the distal lobe of the binding pocket to residues impinging on the stigmatellin binding domain lead to loss of the $g_x = 1.80$ signal, consistent with loss through interference with the binding of Q or QH_2 in this domain. These have variable effects on electron transfer rate. Many of these mutational changes gave resistance to stigmatellin.
2. Changes to residues that project into the cyt ***b***/ISP interface eliminate the $g_x = 1.80$ signal with variable effects on electron transfer. It seems likely that the mutations in this set interfere with the ISP binding, and prevent formation of the complex between Q and ISP_{red} that gives rise to this signal. The variable effects on turnover number would then be explained by the decrease in the residence time of the ISP at the docking interface, and therefore the probability of formation of the reaction complex.
3. Residue changes at positions equivalent to M125, Y132, G137, E272, and F129 led to loss of activity without loss of the $g_x = 1.80$ signal. These cluster at the proximal end of the pocket, closer to the heme b_L, where the pharmacophore of myxothiazol and MOA-type inhibitors bind. Mutations

at all the above residues except E272 show myxothiazol resistance. If the $g_x = 1.80$ signal reflects an interaction between Q and ISP_{red}, then it seems reasonable to conclude that these mutations do not interfere with the binding of either of these species. In line with this, for several of these strains, addition of stigmatellin showed the same EPR line-shape change as seen in wild type. However, mutations at these residues do prevent oxidation of QH_2. The mutations at E272 were particularly interesting from a functional perspective. In the stigmatellin-containing structure 2BCC, E272 forms a H-bond with the inhibitor, and we have suggested that a similar H-bond with the quinol substrate might be formed. From the lack of effect on the $g_x = 1.80$ signal, it seems unlikely that any ligand to the quinone is modified in the mutant strains, suggesting that E272 does not form a ligand to quinone. The loss of a ligand to stigmatellin on mutation of E272 accounts for the otherwise anomalous resistance to this inhibitor, which is in contrast to the myxothiazol resistance for mutation to other residues in this set.

From this analysis, it was suggested that the effects of mutation on inhibitor resistance, function, and the $g_x = 1.80$ signal might have a simple interpretation (222, 223, 232). The $g_x = 1.80$ signal is associated with a complex formed between quinone bound in the Q_o site at the distal end, and the reduced ISP docked firmly at the interface with cytochrome ***b***. The signal is lost whenever this complex cannot form. In the mutant strains in classes 1 and 2 above, mutation interferes with binding of quinone and of ISP, respectively. All liganding interactions between Q_o site occupant and ISP, including formation of the enzyme-substrate complex (ES-complex) between QH_2 and ISP_{ox}, must occur with the occupant in the distal domain. Function may require occupancy of the proximal lobe, as indicated by the overlap between myxothiazol-resistant strains and those in class 3 above.

Mutational Studies of the Movement of the ISP Head

Several recent papers have used mutagenesis to study the movement of the ISP extrinsic domain, or the need for such a movement in function. Suppressor strains that correct mutations in the C-terminal part of the ISP or in cyt ***b*** through mutation in ISP have been interpreted as showing an importance of the hinge region (233–235), and in several studies, the hinge region has been modified directly. These include extensive substitution studies, including changes in length of the hinge region (44, 236–241). In some convincing experiments by Tian et al (237), cysteines have been substituted in pairs at the helical repeat along the sequence that undergoes extension. Oxidation to form a disulfide bridge to freeze the helical configuration led to inhibition of quinol oxidation, which was restored on reduction of the bridge. The membrane anchor is attached to the opposite end of the extrinsic domain from the cluster, so that for the cluster to approach the Q_o site requires the neck region to be extended as the protein pivots. Inhibition by

the disulfide linking could be by preventing the helix from extending, so that the "back end" of the extrinsic domain is held close to the membrane and the cluster cannot pivot into position. However, this interpretation seems inconsistent with results from several labs in the bacterial (44, 238) and yeast (239) systems, which show that the neck can be shortened by three (44, 239) or even five (238) residues and still function. The authors attributed inhibition by the disulfide bridge to an increase in rigidity of the neck region.

While shortening of the neck region is tolerated, extension by even one residue is deleterious, and by more than one, strongly inhibitory (44, 238, 239). Two possible explanations come to mind. The short tether in the wild-type protein may limit the extrinsic domain to a range of positions, from any of which it can rapidly return to its reaction positions. The extra slack provided by the insertion may allow it to reach some conformations from which it cannot readily return. Alternatively, some tension on the tether may be necessary to balance the occupancy of the cyt ***b*** and cyt $\boldsymbol{c_1}$ states—formation of the helix may provide energy to tug the reduced Rieske cluster away from the semiquinone or quinone at the Q_o site. This latter explanation seems more likely, as the inactive mutant with a five-residue insertion shows a typical $g_x = 1.8$ signal (E Darrouzet & F Daldal, personal communication), indicating it is safely docked at Q_o and not stuck in an unnatural position. On the other hand, the 10% active deletion mutant ΔADV (44) showed no $g_x = 1.8$ signal, as if the increased tension on the helix "spring" shifts the equilibrium away from the cyt ***b*** position.

The neck region of the ISP in the $\boldsymbol{b_6f}$ complex seems to be longer and more flexible since it contains at least five glycine residues. However, mild changes in the rigidity of this region in mutants of *Chlamydomonas reinhardtii* in which the six conserved glycines were replaced with alanines failed to modify the properties of the complex (241).

Biophysical Aspects of the Movement of the ISP Head

Xia et al (14) suggested several possible mechanisms to overcome the problem created by the distance between the Fe_2S_2 and heme c_1 centers in their structures. In the Zhang et al (15) structures, the ISP was well enough resolved to limit the options, and we suggested that the ISP head must move during catalysis, since the distances to one or the other reaction partner precluded operation at measured rates in any static configuration. In the four structures for native complexes for which coordinate data are available (14–16), the [2Fe-2S] cluster is in five different positions, corresponding to five different configurations of the ISP head. Positions differing slightly from those in the Zhang et al (15) chicken structure were also reported by these authors for three undeposited structures. These eight configurations suggest that the ISP head is relatively loosely constrained, with particular configurations favored by crystal-packing forces (242). There seems little justification for assigning to any of these native configurations a specific mechanistic role. Rather, they likely reflect the mobility associated with movement. The ISP head

may be tightly constrained only when it is involved in complex formation with substrates or inhibitors. Possible values for association constants under different conditions have been determined from differential electron densities of the mobile head and the rest of the structure (242). The time scale for displacement of the ISP between its two reaction interfaces lies between the diffusion limit at the low end (~25 ns for a 1-D diffusion over 22 Å), and the kinetics of the electron transfer reactions at the high end (~100 μs). The movement is not normally the source of the high activation energy for quinol oxidation (99, 242).

Movement of the ISP under physiological conditions has been demonstrated in *Rb. sphaeroides* by changes in fluorescence energy transfer (FRET) between complementary fluorophores attached to cysteine residues engineered at unique sites on cyt ***b*** and the ISP (232). The results indicate a separation of the proteins as the system becomes reduced, which was not seen in the presence of stigmatellin. Spin interaction between EPR spin probes attached in place of the fluorophores was decreased on addition of decylubiquinol as substrate, but this was inhibited by stigmatellin. Similarly, interaction between a spin probe attached to cyt ***b***, and the spin of the ISP_{red} was diminished by quinol (R Kuras, M Guergova-Kuras, A Smirnov & AR Crofts, unpublished data). In similar experiments, the environment of spin probes attached to cysteines engineered at the ISP docking surface on cyt ***b*** changed on additional of quinol, but not if stigmatellin was present. We interpret these experiments as showing that the oxidized ISP is bound mainly in the cyt ***b*** position, as in the Xia et al (14) structure or the Zhang et al (15) stigmatellin-containing structure. On reduction of ISP, a partial displacement occurred, and movement away from the cyt ***b*** interface was complete when quinone was reduced or quinol added.

Brugna and colleagues (68, 243–245) measured the orientation of the ISP under different redox conditions in a wide range of species. In these experiments, the oriented samples were frozen, and the orientation detected by EPR. In order to detect the oxidized ISP, the sample was irradiated by γ-radiation to reduce the center. These experiments also showed different orientations of the ISP on changing redox conditions. Kramer and colleagues (247; A Roberts, M Bowman, D Kramer, submitted for publication) showed that the environment of Cu^{2+}, bound stoichiometrically to the $\boldsymbol{b_6f}$ complex at an inhibitory site, was modified by the Q_o site occupant (plastoquinol, DBMIB, stigmatellin). They suggested that this reflected participation of the ISP or cyt ***f*** or both in the Cu^{2+} liganding environment, and a change on binding of the ISP at the cyt ***b*** interface.

Israilev et al (248) have simulated the ISP movement using steered molecular dynamics. In these studies, application of a torque around the virtual axis of rotation allowed the extrinsic head to move through the displacement observed between stigmatellin and native structures without significant disruption of the structure. The simulation revealed an interesting sequence of making and breaking of H-bonds between cyt ***b*** and the ISP, and between ISP and cyt $\boldsymbol{c_1}$, which involved conserved residues. These interactions could provide some steerage for the reverse process [formation of the ES- or enzyme-inhibitor complex (EI-complex)] at the

Q_o site. Another interesting feature from this work was a group of water molecules, modeled in the structure as a preliminary to the dynamics calculations, that formed a chain situated in a channel into the protein from the P-side aqueous phase reaching toward the Q_o site. This chain included the heme edge and propionate side chains. It was remarkably stable during the simulation, and crystallographic waters have now been observed in this region in more highly refined structures (S Iwata, personal communication). We have suggested a possible role in proton transfer from the site (169, 223, 248).

Q_o Site Occupancy

In principle, the structures might allow discrimination between single- and double-occupancy models. Structures containing Q_o site inhibitors show occupancy of a bifurcated volume, presumed to be the Q_o site, with different classes of inhibitors occupying different but overlapping domains (14–16, 84, 222). This feature has been interpreted as favoring double-occupancy models (249, 250). The structures support earlier observation on competition between inhibitors (86, 104, 145, 249, 251–256). Class II inhibitors (stigmatellin and UHDBT) bind in the domain distal from heme bL, and interact with the ISP through formation of a H-bond with ISP–His-161, one of the cluster ligands. In contrast, myxothiazol and MOA-type inhibitors (class I) bind in the proximal domain close to heme b_L (14–16, 84, 99, 169, 222). However, the volumes occupied by the inhibitors overlap, because their hydrophobic tails pass out to the lipid phase through a common tunnel. This overlap of occupancy in the tunnel and adjacent volumes explains the exclusive occupancy. Unfortunately, none of the native structures shows any species of quinone occupying the Q_o site, so conclusions about quinone/quinol binding must remain speculative. However, it is clear that although the Q_i site is occupied by quinone, the strongly binding Q_{os} species expected from the Ding et al (165, 224, 225) double-occupancy model is not seen. From quinone extraction experiments, the EPR signal at $g_x = 1.783$ was more resistant to extraction than the Q_i site signal, leading to the prediction that the Q_{os} species would bind more tightly than the quinone at the Q_i site.

Ding and colleagues (165, 224, 225) had shown that either myxothiazol or stigmatellin at a stoichiometry of one per complex could eliminate EPR signals attributed to both Q_{os} and Q_{ow} species. They suggested that either class of inhibitor could displace all quinone from the site. From the architecture of the site, it is difficult to escape the conclusion that any occupant with a "tail," including the native quinone(s), would bind in the same volume as the inhibitors, and would access the site through the same tunnel. The displacement by inhibitors is therefore quite consistent with the structures. Many mutant strains of both bacterial and mitochondrial systems with residue modifications at the Q_o site show differential effects on the binding of the two classes of inhibitors (231). However, none has shown any similar differential effects on the signals attributed to Q_{ow} and Q_{os} species, which would be expected if they bind in the two different domains.

The displacement by binding of one equivalent of either inhibitor, and the lack of any differential effects of mutation, argue against the idea that two quinone species are differentially bound in the two inhibitor binding domains. If the volume of the Q_o site were indeed occupied by two quinones, the structure would have to expand substantially to accommodate the extra occupant in the access tunnel and also in the adjacent volume where the structures would otherwise force a common occupancy. Recent experiments by Sharp et al (250) on inhibition by diphenylamine (DPA) are interesting from this point of view. They showed that, over the 100 μM range, DPA could inhibit quinol oxidation, but not formation of the complex giving rise to the $g_x = 1.80$ or 1.783 bands. As the concentration was raised above that giving inhibition of electron transfer, the $g_x = 1.80$ signal was lost before the 1.783 signal. They interpreted this as showing a triple occupancy of the Q_o site, with DPA binding in a noncompetitive manner in addition to Q_{os} and Q_{ow}. An alternative explanation is that DPA, having no tail, can bind in the proximal domain without causing displacement of quinone bound in the distal domain, but would inhibit electron transfer by competing for occupancy of the proximal domain. Consistent with this, DPA at concentrations in the 100 μM range increased the titer for mucidin, as would be expected if both compete for occupancy of the proximal domain (M Guergova-Kuras & AR Crofts, unpublished information).

The different inhibitor-containing structures show substantial expansion of the site, and changes in configuration upon binding different occupants (99, 232). The expansion suggests that the inhibitors do not displace an existing occupant. However, because of the flexibility, the structures in native crystals might not necessarily represent physiological structures, so the observations above do not exclude double occupancy. It will clearly be of importance in the future to determine the occupancy under physiological conditions.

Activation Barriers in Quinol Oxidation

Activation barriers for reactions of the ***bc*$_1$** complex have been explored in both mitochondrial and bacterial ***bc*$_1$** complexes, with values reported in the range 32–65 kJ mol^{-1}. For mitochondrial systems, recent work has involved assay of the isolated complex under steady-state conditions. In the earlier work Fato et al (257) assayed the rate as a function of [substrate] with either cyt ***c*** or quinol limiting, but the pH was not varied. More recently, Brandt & Okun (228) have measured the steady-state activation energy as a function of pH, and observed a strong dependence, at least in the alkaline range. Paradoxically, over the range in which the activation energy fell with increased pH, the rate also declined rapidly. In photosynthetic bacteria, pre–steady-state kinetics can be measured following flash activation of the complex in situ, and the partial reactions can be distinguished by judicious use of inhibitors, redox poising, and kinetic deconvolution. Crofts & Wang (210) showed that the step with a high activation barrier was after

formation of the enzyme-substrate complex. Since no semiquinone intermediate could be detected, they suggested that the first electron transfer step was limiting, and led to formation of unstable semiquinone. In recent extensions of this work (170, 242, 258), activation energies were measured for each of the partial reactions of the Q_o site as a function of pH over the range 5.5–8.9. No pH dependence was seen in the activation energies of any of the partial reactions contributing to quinol oxidation. Hong et al (170) have discussed the mechanism in the context of the Marcus theory, and the dependence of electron transfer on activation barrier height, reorganization energy, and distance, taking the latter from the structures. Applying the equation suggested by Moser et al (259) to the separate electron transfer reactions, they interpreted their results as providing the following constraints on choice of mechanistic model: (*a*) the activation barrier is after formation of the enzyme-substrate complex; (*b*) the activation barrier is not determined by dissociation of any group with a pK in the physiological range or higher; (*c*) the highest activation barrier, $\sim$65 kJ mol^{-1}, is in the first electron transfer from quinol to ISP_{ox} leading to formation of semiquinone; (*d*) the intermediate semiquinone is not the activated state.

From their results, two scenarios for the role of intermediate states seemed plausible for single-occupancy models.

1. A modified Link (219) mechanism in which dissociation to products occurs after the second electron transfer. In this type of mechanism, since the second electron transfer has to occur over the 11-Å distance from semiquinone bound in the distal domain of the Q_o site to heme b_L, realistic mechanisms require a high occupancy of the intermediate state. Since no semiquinone is detectable, a plausible case requires demonstration that the ISP_{red} and semiquinone are formed, but undetected by EPR, under conditions of oxidant-induced reduction.
2. A modified Crofts-Wang (169, 210, 223) mechanism, with dissociation to products after the first electron transfer. This model is in line with the evidence showing that semiquinone is undetectable (210, 215). However, the low occupancy of semiquinone would likely necessitate movement of the semiquinone to the proximal domain to allow rapid reduction of heme b_L in the second electron transfer reaction. Such a movement has not been demonstrated but is compatible with evidence from the structures and the consequences of mutation (165, 223–225, 231, 232, 256), showing a critical role for residues lining the proximal domain.

For double-occupancy models, the critical parameters would be model dependent. Since none of the solved structures for the native complex show any occupant nor could any accommodate two quinone species without considerable distortion, they do not provide dependable distance information. However, it is clear that double occupancy could allow an extra redox center in any path, and so overcome difficulties arising from too long an electron transfer distance.

The pH Dependence of Quinol Oxidation

Both in steady-state experiments with mitochondrial complexes, and in pre–steady-state measurements following flash illumination of bacteria, a strong pH dependence for the rate of quinol oxidation is observed. In experiments over a wide pH range, Link, Brandt, and colleagues (228, 260) showed an increase in steady-state rate over the acidic range, and a decrease over the alkaline range, with a maximal rate at neutral pH. A similar pH dependence for rate of quinol oxidation following flash excitation was seen in *Rb. sphaeroides* (169, 170, 258). Brandt et al (228, 229) interpreted the pH dependence in terms of a kinetic model in which the rate depended on dissociation of a group with pK of ~6.5, and association of a group with pK of ~8.5. Ugulava & Crofts (261), Crofts et al (169, 170, 258), and Snyder & Trumpower (246) noted that the pH dependence in the acid range could be explained by the pK of ~7.6 attributed to dissociation of His-161 of the ISP (74, 219), one of the cluster ligands, if the dissociated ISP_{ox} were required for formation of the enzyme-substrate complex at the Q_o site. This suggestion has been supported by the observation of a shift to higher value in the pH profile for quinol oxidation in a strain of *Rb. sphaeroides* mutated in the ISP (Y156W strain) in which the pK was shifted to a higher value (pK of ~8.5) (169, 170a). The difference between the pK of ~7.6 in wild type (or mitochondrial complexes), and the apparent pK for quinol oxidation rate (pK_{app} of ~6.3–6.5), was explained in terms of the additional equilibrium constant involved in formation of the enzyme-substrate complex, which would pull the dissociation reaction over toward the dissociated form under functional conditions (170).

A Possible Mechanism for Quinol Oxidation

A possible mechanism for the Q_o site (169, 223) is illustrated in Figure 8. First, oxidizing equivalents are transferred to the site through cyt $\boldsymbol{c_1}$ through a movement of the ISP between reaction domains on cyt $\boldsymbol{c_1}$ (ISP_C configuration) and on cyt $\boldsymbol{b}$ (ISP_B configuration) (15, 99, 232, 242).

As seen in Figure 8*A,* the reaction proceeds from an ES-complex involving ISP_{ox} docked at the P-side external interface on cyt $\boldsymbol{b}$, and bound ubiquinol at the distal end of the Q_o site pocket (169, 261). Quinol is H-bonded by His-161 of the ISP and Glu-272 of cyt $\boldsymbol{b}$.

Electron transfer from QH_2 to the ISP leads to formation of semiquinone (*process 1*), and dissociation to products (*processes 2, 5*), in the step with a high activation barrier (170, 210). Because ISP acts as an H-carrier, this leads to separation of $H–ISP_{red}$ (*process 2*), which moves to the ISP_C site for oxidation, and release of the first H^+ (Figure 8*B, process 7*).

The semiquinone rotates in the pocket into the proximal end (*process 5*), near heme b_L, which facilitates its rapid oxidation (Figure 8*B*). The movement of semiquinone to the proximal domain would insulate it from further reaction with the reoxidized ISP, or with O_2, and thus minimize the decoupling of electron transfer, or formation of superoxide anion. Next, the semiquinone passes its

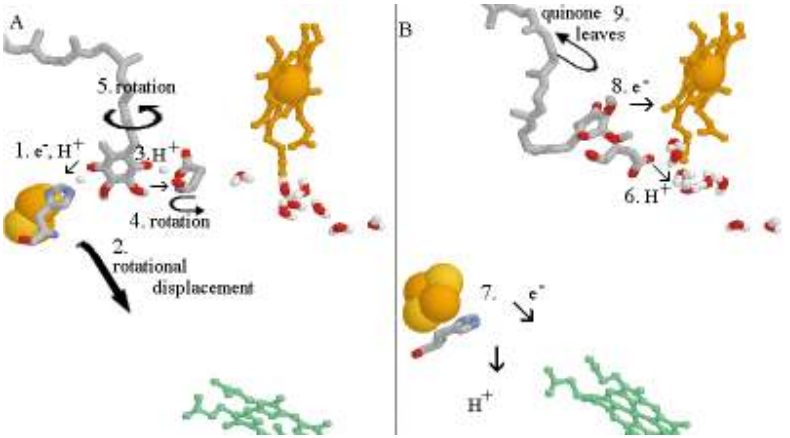

Figure 8 The proposed mechanism for reactions at the Q_o site after formation of the reaction complex. Numbers indicate the sequence of reactions. In the text, the italic process numbers refer to reactions numbered in the figure.

electron to the cyt b_L heme (*process 8*), and thence to heme b_H, and the Q_i site, and the quinone exits the Q_o site (*process 9*).

At some point between *processes 2* and *8,* the second proton is released. We show this as occurring through protonation of the Glu-272 carboxylate side chain by the neutral semiquinone (*process 3*), to give the semiquinone anion. Rotation of the Glu-272 side chain (*process 4*), followed by dissociation, provides a pathway for exit of the H^+ via a water channel to the external aqueous phase (*process 6*) (169, 223, 248).

Meanwhile, the ISP_{ox} can return from cyt $\boldsymbol{c_1}$ by the tethered diffusion mechanism and initiate another turnover of the Q_o site.

Uncoupling of the Bifurcated Reduction of cyt *f* and cyt b_6 in Chloroplasts

An apparent uncoupling of the bifurcated flow of electrons from the Q_o site to cytochromes ***b*** and the high-potential chain has been observed in $\boldsymbol{b_6f}$ complexes where, in certain cytochrome ***f*** mutants with retarded reduction of cyt ***f***, reduction of cyt ***b*** is not retarded and seems to occur first (263). A similar result has been seen with some N-terminal mutants of *Chlamydomonas* cyt ***f*** (J Fernandez-Velasco, personal communication).

In the wild type, following flash activation with the system initially poised so that plastocyanin, cytochrome ***f***, and the Rieske protein are reduced, and cytochrome ***b*** oxidized, plastocyanin becomes oxidized via photosystem I on a μs time scale, and rapidly equilibrates with cytochrome ***f***. Then cytochrome ***b*** is reduced and cytochrome ***f*** is re-reduced with a similar time course, as expected from

the concerted electron transfers of the bifurcated reaction. Under many conditions, since the Rieske is invisible in spectrophotometric experiments, some departure from this ideal situation occurs because of the rapid equilibration among the high-potential components, and their relative E_m values. In addition, depending on redox poise, electron flow out of the cyt ***b*** chain occurs, truncating the kinetics. Deconvolution is needed to sort out the complications (264–266).

In the framework of the Q-cycle, the stimulus that initiates turnover of the Q_o reaction and cyt ***b*** reduction after the flash is arrival of an oxidized ISP at the cyt ***b*** position. This can occur only after oxidation of the ISP by cyt ***f***, i.e. after re-reduction of cytochrome ***f***. Thus flash-induced reduction of cyt ***b*** preceding re-reduction of cytochrome ***f*** does not fit naturally into the Q-cycle scheme as currently formulated. Cramer and coworkers (204) suggested that plastocyanin may react directly to oxidize the ISP, triggering turnover of the Q_o site before oxidizing equivalents could arrive via the mutated cyt ***f***.

Mechanism of Quinone Reduction at the Q_i site

In the modified Q-cycle, the Q_i site operates through a two-electron gate mechanism, in which the reduction of quinone is accomplished by successive electron transfers from heme b_H, itself reduced by successive turnovers of the Q_o site (9, 143, 208, 216, 217).

$$\text{E.cyt } b_H + Q \leftrightarrows \text{E.cyt } b_H.Q \xrightarrow[e^- \text{ from } Q_o\text{-site}]{} \text{E.cyt } b_H^-.Q \xrightarrow[H^+]{} \text{E.cyt } b_H.Q^-\cdot[H^+]$$

$$\text{E.cyt } b_H.Q^-\cdot[H^+] \xrightarrow[e^- \text{ from } Q_o\text{-site}]{} \text{E.cyt } b_H^-.Q^-\cdot[H^+] \xrightarrow[H^+]{} \text{E.cyt } b_H.QH_2 \leftrightarrows \text{E.cyt } b_H + QH_2.$$

Berry et al (92) modeled the quinone with ligation by His-202, Ser-206, and Asp-229, shown by mutational studies to play a critical role (231, 267–269), and suggested a mechanism based on this pattern of ligation, in which the dissociable groups play a specific role in proton processing at the site. Antimycin is the classical inhibitor, and the structures now show plainly that the inhibitor displaces quinone from its binding site, as had been generally assumed. The pattern of ligation is different for antimycin than quinone, accounting for the many mutant strains that show resistance to the inhibitor without impaired function.

The physicochemical parameters defining operation of the site have been explored though kinetic spectrophotometry, redox titration using spectrophotometry of heme b_H, and EPR spectroscopy of both the heme and the semiquinone intermediate. Because the reactions at the Q_o site are limiting, rate constants for partial processes associated with the forward reaction at the Q_i site (electron transfer through the ***b***-heme chain to the site occupant), cannot be directly measured

except in mutant strains with slowed kinetics, although estimated limits have been suggested (143, 210, 216, 217). Equilibrium constants for oxidation of cyt b_H depend on redox state, with some suggestion that reduction of quinone is less favored than reduction of semiquinone. Kinetic parameters for the reverse reaction can be measured following substrate addition in the presence of myxothiazol to inhibit oxidation of quinol at the Q_o site, or in chromatophores following illumination with the pool initially oxidized (270, 271). Redox titrations of cyt b_H in the absence of antimycin show two components, with redox midpoint potential (E_m) values of 50 and 150 mV. The higher-potential component, cyt ***b***-150, is lost on addition of antimycin, and its amplitude appears in the 50 mV component (270–274). When chromatophores or the isolated complex are poised at $E_h \approx 100$, where the 150 mV and 50 mV components are predominantly reduced and oxidized, respectively, addition of antimycin induces an oxidation of the cyt ***b***-150 component (272).

Two different types of explanation have been offered for this ***b***-150 phenomenon. In the first, Salerno (273) and Rich and coworkers (274) propose that the midpoint potential of cytochrome b_H depends on the redox state of the quinone at the Q_i site. Rich et al (274) proposed a set of ΔG values in a minimal eight-state system that provided a good fit to the data. A second mechanism (270, 272, 275) suggests that the ***b***-150 form is generated by reversal of the second electron transfer of the normal forward reaction. A single equilibrium constant, calculated from the E_m values for the components involved, then provided a good fit to the data. This mechanism also provides a natural explanation for the antimycin-induced oxidation of cytochrome ***b*** (272) and the coupled appearance of semiquinone and ferroheme $\boldsymbol{b}_H$ on reduction of the complex in the presence of myxothiazol (143, 272). The mechanism invokes only interactions demonstrated by experiment. It assumes that heme $\boldsymbol{b}_H$ equilibrates via one-electron reduction by ubiquinol with formation of semiquinone, but is not in two-electron equilibrium with the Q-pool, or in equilibrium with the mediators at the low concentrations used in spectrophotometric experiments. However, the E_m values for the Q_i site semiquinone couples, and the differential binding of Q and QH_2, were taken from EPR titrations, on the assumption that the disproportionation reaction reached a natural equilibrium through mediators at the high concentrations used in these experiments.

These two mechanisms make different predictions for the titration profile of the semiquinone relative to that of ***b***-150, and might be distinguished by potentiometric titrations monitored by optical and EPR spectroscopy (276). However, such experiments might be complicated by the possibility that the unpaired spins of the semiquinone and oxidized b_H might couple and become EPR-silent (276, 277). Another fundamental difference is the assumption of the second model that cytochrome b_H does not equilibrate directly with the mediators at low concentration. Given that small water-soluble redox reagents do react with cyt ***b*** (142), it should be possible, by using high concentrations of one-electron mediators of the appropriate E_m, to demonstrate a relaxation of the coupling of the semiquinone redox state and that of heme b_H implicit in the second mechanism. Since the first explanation

assumes the heme is in equilibrium with the electrodes and the heterogeneous titration is due to actual changes in the midpoint potential, the results would be the same with high or low mediator concentration unless the mediator displaced quinone from the Q_i site.

Electron Transfer Between Monomers

The relatively short distance between the heme b_L groups of the two monomers has raised the question of the possibility of electron transfer between them (14), since the 7.9 Å between vinyl groups would be expected to favor an intrinsic rate constant in the submicrosecond range. If electron transfer occurred rapidly, it would allow full reduction of heme b_H following flash-excitation in the presence of antimycin when one of the Q_o sites of the dimer was inhibited. Such an effect should be easily detected in the kinetics of cyt b_H reduction on titration with myxothiazol or stigmatellin, but neither sigmoidicity in the titration curve nor any marked biphasic kinetic is seen (222). On the other hand, nonlinear antimycin titration curves (278) might be interpreted as evidence for such crossover.

PHYLOGENETIC AND EVOLUTIONARY CONSIDERATIONS

Currently available sequences for bacterial and archaeal cyt ***b*** and Rieske ISP were retrieved from the National Center for Biotechnology Information (NCBI) protein database. In our analysis for the $\boldsymbol{bc_1/b_6f}$ family, we have used only a few representatives from the mitochondrial $\boldsymbol{bc_1}$ and the chloroplast $\boldsymbol{b_6f}$ complexes since they show high similarity in each respective group (138, 279). Only organisms for which both the cyt ***b*** and the ISP sequences were available were used. Additionally, the genomes currently being sequenced were searched using the Blast 2.0 engine. A sequence of 35 residues in the region of the highly conserved –PEWY– loop was used to search for cyt ***b*** orthologs. The search was performed several times using the homologous sequences from different phyla to avoid bias. Similarly, for the ISP, a sequence of 40 residues in the cluster binding region containing the conserved CTHLGC(X_{11-24})CPCH was used to search the databases. The contigs in which either one of the two proteins were identified were subsequently translated into six open reading frames and searched for the presence of the other two proteins. The sequences for cyt ***b*** and the ISP could be easily identified and they were clustered together in all cases, whereas homologs for cyt $\boldsymbol{c_1}$ could only be assigned with some ambiguity. If a cyt ***c*** binding signature CXXCH was found in an open reading frame (ORF) in the immediate vicinity of the cyt ***b***/ISP cluster, the corresponding ORF was tentatively assigned to a cyt $\boldsymbol{c_1}$. The rationale behind this approach rests on the assumption that clustering of genes in operons is a good indicator for the physical interaction of the expressed proteins into complexes (280). No cyt ***c*** analog was found in the vicinity of the ISP/cyt ***b*** cluster in *Chlorobium tepidum*. This is consistent with a previous report about *Chlorobium limicola* where the

transcriptional unit contained only ISP and cyt ***b***. Since *C. tepidum* contains a cyt ***c*** encoded elsewhere in the genome, it is possible that it may interact with the ISP/cyt ***b*** subcomplex in a manner similar to that described for *C. limicola* (281).

Phylogeny of cyt *b* Subunits

Figure 9 shows transmembrane helix prediction for three widely divergent cytochromes ***b***. Note the N-terminal extension on *Chlorobium* cytochrome, the C-terminal extension on *Mycobacterium,* and the lack of helix H in *Chlorobium*.

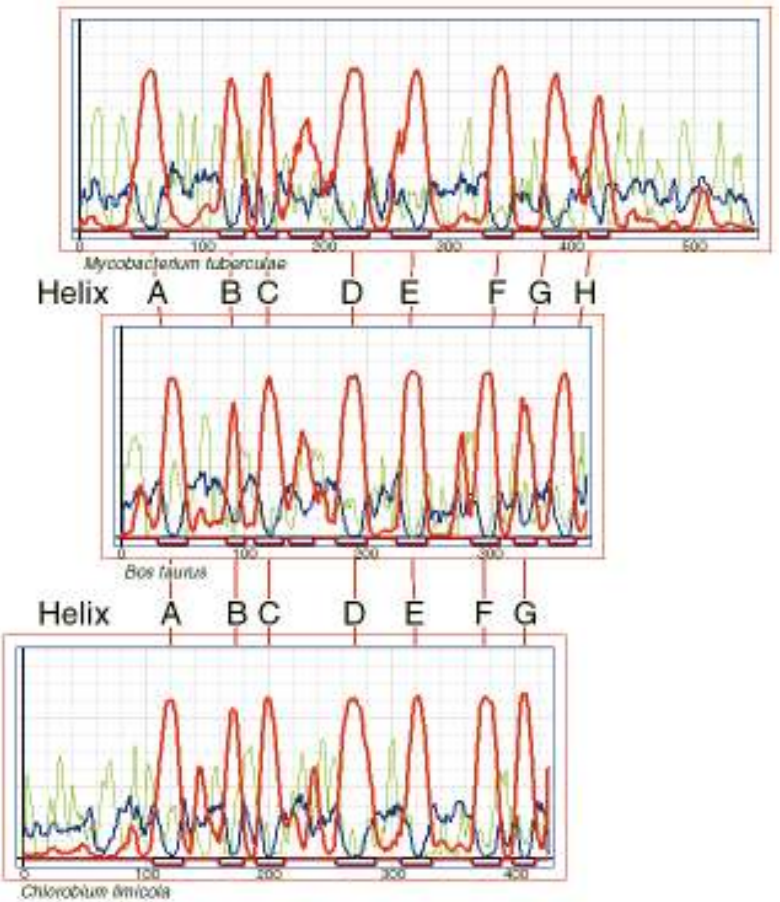

Figure 9 Transmembrane helix prediction for cytochrome ***b*** from *Mycobacterium,* beef, and *Chlorobium. Red line*, transmembrane helix preference; *blue line*, beta preference; *green line*, modified hydrophobic moment index (see Reference 282). *Dark red line* (below abscisa), predicted transmembrane helix position. Calculated by methods in Reference 282 using default parameters by the WWW server at http://drava.etfos.hr/~zucic/split.html.

Note also that even with state-of-the-art prediction methods, an extra transmembrane helix is weakly predicted between helices C and D in two of the three sequences.

An alignment for the multiple species was produced for the cyt ***b*** sequences, including three chloroplast and eight mitochondrial samples, with representatives of the main eukaryotic families. When cyt ***b*** was present as two polypeptides, the sequence of an artificially fused protein was used. Figure 10*a* shows the phylogenetic tree deduced from the resulting alignment (alignments for a subset of cytochrome ***b/b*$_6$**-IV sequences are available in the supplementary materials deposited on the Annual Reviews Web site at http://www.AnnualReviews.org). The root of the tree was chosen as the separation of the archaeal (*Sulfolobus*) and the eubacterial sequences. The sequences appear to be orthologous and the major branching pattern can be assumed as correct at 95% certainty, since the bootstrap values supporting it are higher than 70 (284). However, the separation of *Aquifex* from the *Chlorobiaceae* should be considered with caution since the bootstrap value is only 43. The tree topology is in good agreement with the evolutionary tree based on the sequences of 16S rRNA (Figure 10*b*). All of the different subclasses are clustered together, with the epsilon subgroup as the most deeply rooted. The internal branching in the group of the beta and gamma proteobacteria shows lower bootstrap values, making conclusions as to the evolution of the protein in this subgroup difficult. The alpha subdivision of the proteobacteria is shown as the closest ancestor of the mitochondria in accordance with the current evolutionary models. The tree is also in good agreement in positioning the cyanobacteria as the closest ancestor of the chloroplast. An important difference from the 16S rRNA tree concerns the close relationship between cytochromes ***b*** from proteobacteria and *Aquifex*. Indeed, the latter appears to be the direct ancestor of proteobacteria.

The tree, based on overall sequence similarity, does not take into consideration the currently available structural and functional information. Since the structure is known for one member, the mitochondrial ***bc*$_1$** complex, it is interesting to choose a few features of known structural significance and see how they correlate with the evolutionary trees. Table 8 compares four features that distinguish ***b*$_6$**-IV complexes from mitochondrial ***bc*$_1$** complexes. The first is the number of residues (exclusive) between the conserved histidine heme ligand in transmembrane helix D, which is 13 in the ***bc*$_1$** complex and 14 in the ***b*$_6$*f*** complex. This can be expressed as a 14- versus 15-residue interval between the heme ligands. The 14-residue interval seen in the ***bc*$_1$** complexes is a multiple of the heptad repeat observed in coiled coils and nearly a multiple of the 3.6 residues per turn of α helix. This puts the two histidines on top of each other in a helical-wheel plot, as is actually observed in the structure. Since no atomic-resolution structure is available yet for a ***b*$_6$*f***-type complex, it is not known whether the extra residue affects the relative positions of the heme ligands, or is accommodated by a π bulge (285) without disturbing the rest of the helix. Among *Eubacteria*, only the α proteobacteria have the mitochondrial arrangement. Subclasses β, γ, and ε of the proteobacteria (with the exception of one γ representative, *Allochromatium vinosum*) as well as *Aquifex,*

TABLE 8 Correlation of four cyt b/b_6 features of known structural significance over a wide phylogenetic range

B/D-spacing[a]	Q_i-ligand[b]	b/b_6[c]	PEWY[d]	Organisms
13/13	E	b	P(PD)W(YF)	Craenarchae (*Sulfolobus, Aeropyrus*)
13/13	H	b	PEWY	α proteobacteria + mitochondria
13/13	H	b	PVWY	γ proteobacterium *A. vinosum*
13/14	H	b	PVWY	β and γ proteobacteria
14/14	R	b	PEWY	*Aquifex*
13/14	R	b	PEWY	ε proteobacteria
13/14	R	b_6	PEWY	Cyanobacteria, chloroplasts
13/14	R	b_6	PDWY	*Bacillus, Heliobacillus*
13/14	Q	b	PEWY	*Chlorobium*
13/14	?	b	PDWY	*Deinococcus*
13/14	?	b	PD(WF)Y	*Mycobacterium, Streptococcus*

[a] The number of residues between conserved heme-binding histidines in transmembrane helices B and D.

[b] The type of residue at the position that aligns with H202 of yeast bc_1 complex, the Q_i ligand.

[c] Single (***b***) or split (b_6) cyt ***b***.

[d] Sequence aligning with PEWY (residues 271–279) of yeast cyt bc_1, involved in the Q_o site.

Chlorobium, and all the firmicutes have the heme ligands of helix D separated by 14 residues; interestingly, *Aquifex* also has the heme ligands in helix B separated by 14 residues. The three archaeal sequences have 13 residues in both helices as in the mitochondrial cytochrome. Two of these are from *Sulfolobus acidocaldarius*, and seem to function as parts of quinol oxidase complexes which, unlike the bacterial quinol oxidases, combine the functionality and the proteins of a cyt bc_1 complex and a cytochrome oxidase (58).

A second characteristic is the type of residue that aligns with the highly conserved H202 in yeast mitochondrial bc_1, which has been shown to be a ligand for quinone at the Q_i site. Of those cytochromes that have 13 residues between the helix D heme ligands, all the eubacterial ones have H as in mitochondria, but the three archaeal cytochromes have E. The b_6f ligand R is present only in cytochromes that have 14 residues between helix D heme ligands. Besides the chloroplast and cyanobacterial complexes, R is present in *Aquifex*, the ε proteobacteria, and the b_6f-like firmicutes *Bacillus* and *Heliobacillus*. The firmicutes *Mycobacterium, Streptomyces*, and *Deinococcus* have very little homology with bc_1 or b_6f complexes in the DE linker, so it is difficult to assign a residue, if there is any, that serves as a ligand for Q_o in place of the mitochondrial H202. *Chlorobium* has Q in place of this residue.

A third characteristic is the split ***b*** arrangement of chloroplasts, with sequences homologous to mitochondrial cyt ***b*** divided between a shorter cyt b_6 containing helices A–D, another subunit containing helices E–G, and no homolog of helix

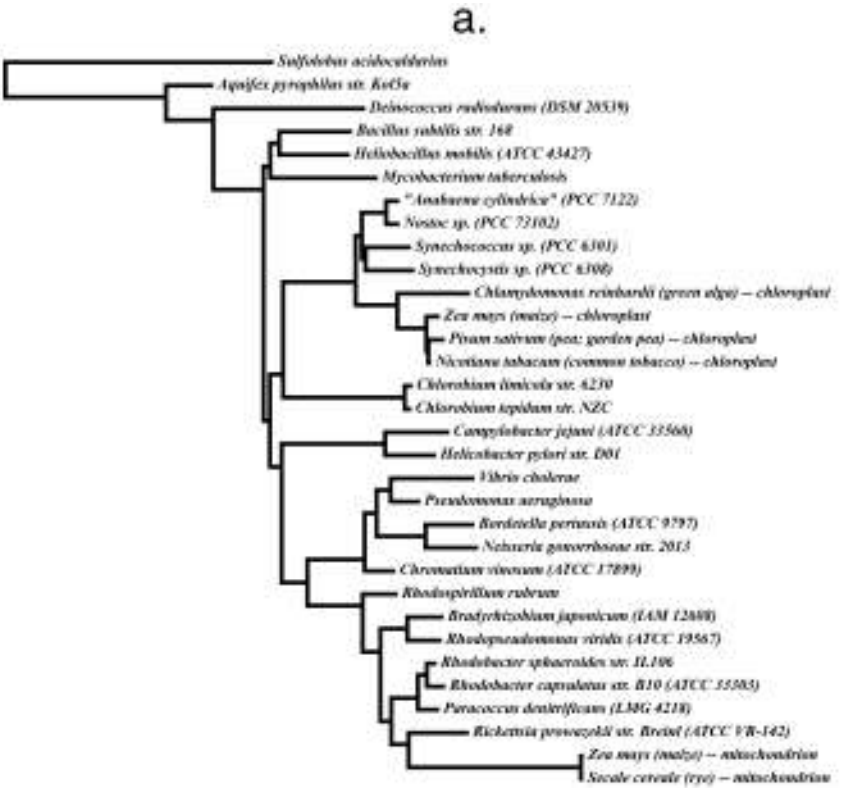

Figure 10 (*Continued*)

H. This arrangement is seen only in cytochromes with 14 residues between helix D heme ligands and with R as the Q_o ligand in place of H202; specifically in the *Bacillus*-like firmicutes and the cyanobacterial and chloroplast $\boldsymbol{b_6f}$ complexes. In *Bacillus* the subunit with helices E–G has a ***c*** cytochrome appended to the C terminus, which may serve the function of cyt $\boldsymbol{c_1}$, as discussed later. This requires the cytochrome to be on the periplasmic or P-side of the membrane, which would not be the case if cyt ***b*** helix H were present.

The fourth characteristic is the conserved PEWY sequence, which is structurally important for the formation of the Q_o site. The Glu of this sequence (272 in the yeast sequence) was shown to provide a ligand to the Q_o site inhibitor stigmatellin (169, 223) and to be functionally important in both purple bacteria (169) and chloroplast (286). It is therefore interesting to note the substitution of this residue by a valine in the case of β and γ subclasses of proteobacteria. Additionally, one *Sulfolobus* gene and the similar *Aeropyrus* sequence have PPWF in place of PEWY and so may be quite unusual in the Q_o site. The other *Sulfolobus* gene has the more conservative PDWY.

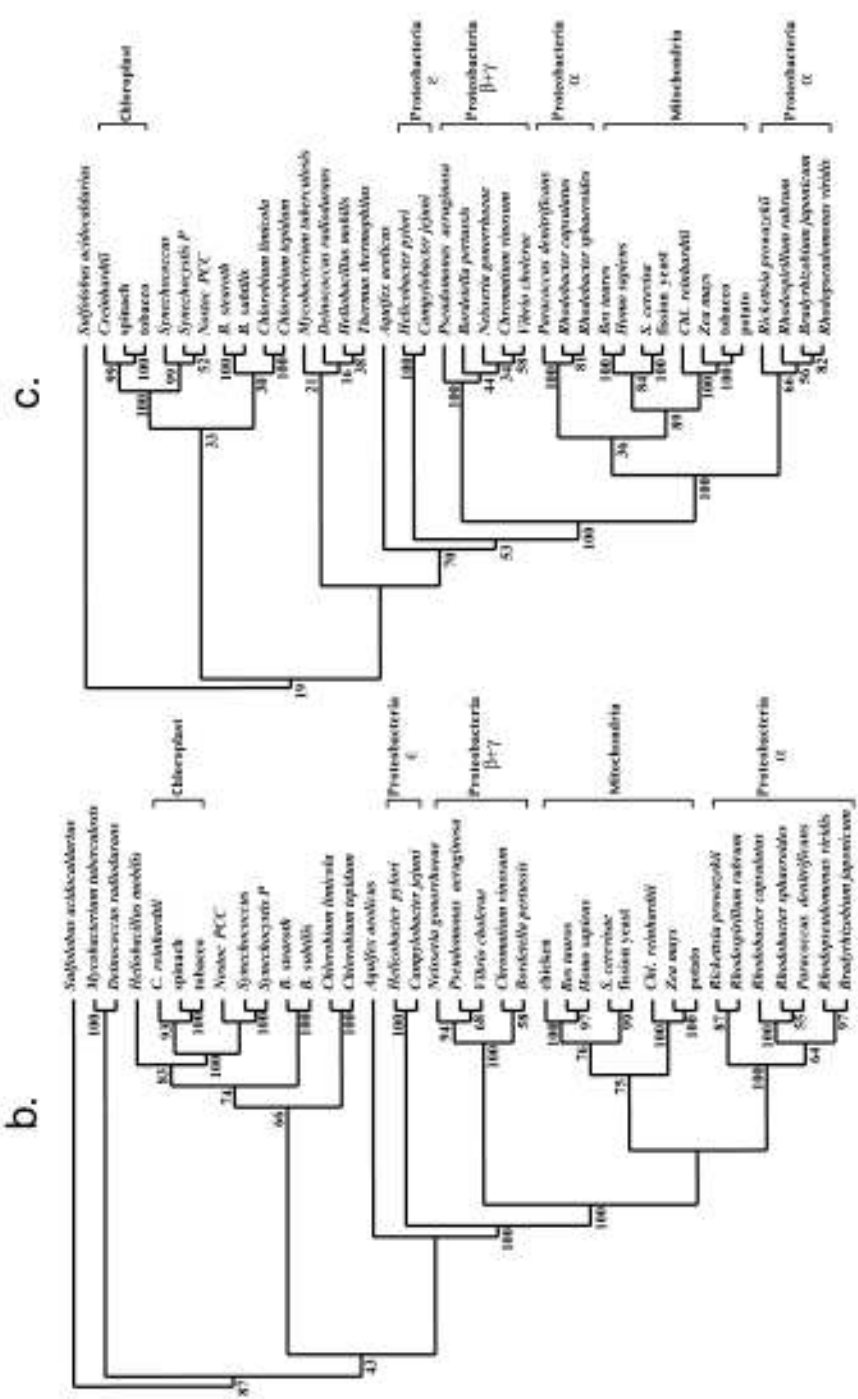

Figure 10 Phylogenetic trees based on (*a*) 16S rRNA, (*b*) cytochrome ***b***, and (*c*) the Rieske ISP. Details are provided in the text.

These characteristics do not internest perfectly to allow scenarios in which each change occurred only once. All complexes with the split cytochrome ***b*** have R as the Q_i ligand, and all complexes with R as Q_i ligand have 14 residues between helix D heme ligands. This would suggest that splitting of cytochrome ***b*** is more recent than choice of the Q_i ligand, which is more recent than insertion/deletion of a residue in helix D. However, while the large group with H as Q_i ligand has mainly 13 residues between helix D heme ligands, the β, ε, and some γ proteobacteria have 14. This suggests that insertion or deletion of a residue in helix D must have occurred more than once. If so, that would also avoid the problem of classifying α proteobacteria with the archaea, and ε, β, and γ proteobacteria and *Aquifex* with firmicutes and cyanobacteria; comparison based on the whole sequence suggests the opposite. The choice of residue X in –PXWY– has been made independently at least three times, in 14-residue complexes with cyt ***b*** split or unsplit and within 13-residue complexes. Further difficulties in relating the tree derived from 16S rRNA sequences with either the above scenario or one based on comparing whole sequence might be attributed to lateral gene transfer.

Phylogeny of the Iron-Sulfur Protein

The alignment of the Rieske sequences included 38 sequences, three of which are chloroplast and eight mitochondrial. The alignment showed a very well conserved C-terminal region containing the ligands for the iron-sulfur center. The N-terminal segment showed a low degree of conservation. Hydropathy analysis showed that all of the sequences contain a hydrophobic span at the N-terminal end, starting with a well-conserved RR (or KR) motif (see alignment on the Annual Reviews web site at http://www.AnnualReviews.org). The hydrophobic spans were aligned, although they do not seem to show any significant conservation. Additional modifications, reflecting the structural homology observed between the chloroplast and mitochondrial ISP (72) were also introduced in the alignment. The tree generated from this alignment is shown in Figure 11. The overall branching topology is similar to that of cyt ***b***, though some of the branching patterns are supported by lower

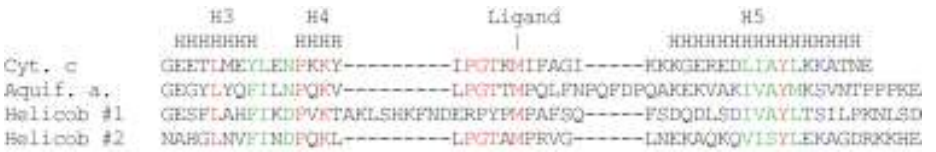

Figure 11 Sequence homology between *Aquifex* and *Helicobacter* cytochromes and mitochondrial cyt ***c*** in the region from helix H3 to H5. The designation of helices and methionine ligand in the top two lines is based on the structure of cyt ***c***. Sequence identifiers are: Cyt. c, bovine mitochondrial cyt ***c***; Aquif. a, cytochrome from *Aquifex aeolicus*; Helicob #1 and #2, domains 1 and 2 of the *Helicobacter pylori* diheme cytochrome.

bootstrap values reflecting the numerous deletions and insertions included in the alignment. The proteobacteria in the ISP tree are grouped together with similar topology to the cyt ***b*** tree, and once again *Aquifex* appears as their closest ancestor. Since the branches separating *Mycobacteria*, *Deinococcus*, *Heliobacillus,* and *Thermus* are supported by very low bootstrap values, they cannot be considered with the same certainty.

Phylogeny of the cyt *c* Subunit

Unlike cyt ***b*** and the Rieske iron-sulfur protein, which show sequence homology throughout these diverse ***bc*** complexes, the associated type ***c*** cytochromes show significant homology only within limited domains. Structures are available for mitochondrial cyt $\boldsymbol{c_1}$ and the chloroplast cyt ***f***, and the basic folds of the two proteins are completely different. A search for sequences similar to bovine cyt $\boldsymbol{c_1}$ or spinach cyt ***f*** among *Eubacteria* yields only proteobacteria for cyt $\boldsymbol{c_1}$ and only cyanobacteria for cyt ***f***. There are ***c***-type cytochromes associated with ***bc*** complexes in the other groups, but they are too dissimilar to be identified by homology with cyt $\boldsymbol{c_1}$ or ***f***. In some cases they have been identified by isolating and characterizing the complex. More examples can be obtained by searching the database for cyt ***c*** heme-binding signature sequences. As a rule, all ***c*** cytochromes have the heme bound covalently by thioether linkages between the vinyl groups of protoporphyrin and two cysteine residues separated in the amino acid sequence by two residues and followed by the axial-liganding histidine, giving the characteristic motif CXXCH. The complexity of this motif is not great enough to avoid a lot of false positives, but when combined with other information such as occurrence in the vicinity of cyt ***b*** and Rieske sequences, it is highly suggestive of a ***c*** cytochrome associated with a ***bc*** complex.

By far most of the known ***c*** cytochromes, including cyt $\boldsymbol{c_1}$ but not cyt ***f***, belong to what Ambler has defined as class I cytochromes. The heme is bound to cysteines and histidine near the N-terminus of the protein; usually (if not always) the other axial ligand is a methionine about 3/4 through the chain, and there is sequence homology with the horse heart cyt ***c***. A great deal of sequence data is available now for ***c*** cytochromes, and quite a few atomic-resolution structures have been determined. All of the class I cytochromes proved to be largely α-helical in secondary structure, and the arrangement of three of the helices is conserved both as to their order in the polypeptide chain and their relative positions in three dimensions.

Since most of the ***c*** cytochromes belong to class I, and since cyt $\boldsymbol{c_1}$ but not cyt ***f*** is a class I cytochrome, it is not surprising that the ***c*** cytochromes associated with most of the $\boldsymbol{bc_1}$ complexes appear more similar to cyt $\boldsymbol{c_1}$ than to cyt ***f***. A reasonable nomenclature that emphasizes the function of the cytochromes would be to classify all class I cytochromes functioning in ***bc*** complexes as cyt $\boldsymbol{c_1}$. Traditionally cytochromes have been classified by structure, however, and if one of the new cytochromes is less similar to cyt $\boldsymbol{c_1}$ than other class I cytochromes that

have already been classified as separate families, it might be better not to call them all cyt $\boldsymbol{c_1}$. This problem can be better addressed after more of the divergent ***bc*** complexes have been characterized structurally and functionally. For the time being, we will refer only to "class I cytochromes associated with ***bc*** complexes" unless they share a number of features with cyt $\boldsymbol{c_1}$ that are not present in all other class I cytochromes.

A search for class I cytochromes associated with ***bc*** complexes, as described above, led to the assignment of six heme C–containing sequences in the genomes of six species. Additional sequences containing a ***c***-type heme-binding motif were retrieved from the complete genomes of *Aquifex, Mycobacterium,* and *Helicobacter*. Although these sequences were not previously explicitly assigned to the cyt $\boldsymbol{c_1}$ moiety of $\boldsymbol{bc_1}$-type oxidoreductases, they were assumed as such and included in this study. The hydropathy profiles of all the sequences showed a transmembrane helix at the C terminus, which is characteristic for cyt $\boldsymbol{c_1}$. The sequences from *Bordetella, Neisseria, Pseudomonas,* and *Vibrio* showed similarity in the range of 50%–70% to the cyt $\boldsymbol{c_1}$ sequence from *Chromatium vinosum,* thereby validating our initial assignment. The similarity of the *Aquifex* and *Deinococcus* sequences were lower (20%–30%) but still in the range necessary to confirm some analogy to the proteobacterial cyt $\boldsymbol{c_1}$.

Four of the 22 sequences used in this study contain two-heme binding regions: *Mycobacterium, Heliobacillus, Helicobacter,* and *Campylobacter*. The diheme protein encoded by the petA gene from *Heliobacillus mobilis* has already been assigned as a part of a $\boldsymbol{b_6/c}$-type complex of menaquinol-cyt ***c*** oxidoreductase (132a). Detailed analysis of the sequences from *Campylobacter* and *Helicobacter* showed an internal homology between the two-heme binding regions, probably resulting from a gene duplication. The second part of the protein, containing the C-terminal transmembrane helix, showed more than 30% similarity with the rest of the proteobacterial sequences. Such an internal similarity is not found in the other two diheme cytochromes of *Mycobacterium* and *Heliobacillus*.

Without structural information and with insignificant sequence homology, we depend on motifs to say whether a given ***c*** cytochrome is related to cyt $\boldsymbol{c_1}$, cyt ***f***, or should be classified as a separate type. From the examples where structures are available, we can chose motifs that reflect structural characteristics, and thus make assumptions about the cytochromes for which we have only sequence information. We have attempted to choose motifs to identify the most highly conserved regions of class I cytochromes, and thus determine the lengths of the variable linker segments between these landmark conserved sites. The different subclasses of class I cytochromes can then be characterized based on the length of the various segments. While such a detailed analysis is beyond the scope of the present work, we will point out that cytochromes $\boldsymbol{c_1}$ are characterized (among other things) by a long segment (50–70 residues) between the heme-binding motif (CXXCH) and the heme-bracing motif [GP]P[NDEAS]L. From the structures of vertebrate cytochrome $\boldsymbol{c_1}$, this segment contains the Y-loop, one branch of which folds back against the core of cyt $\boldsymbol{c_1}$ and contains acidic residues implicated in binding of cytochrome ***c***. The other

branch of the Y-loop reaches out and contacts cytochrome $\boldsymbol{c_1}$ in the other monomer of the dimer. Besides mitochondrial cytochromes $\boldsymbol{c_1}$, such a long segment is found in all the proteobacterial cytochromes except the *Helicobacter* diheme cytochrome, and is found in the *Aquifex* cytochrome. All of the firmicutes have short segments here, and so are likely to be quite different from cytochrome $\boldsymbol{c_1}$ structurally. Even *Aquifex* and *Helicobacter* show more resemblance to cytochrome ***c*** than cyt $\boldsymbol{c_1}$ in the region of helices H3–H5. Figure 11 shows the alignment of these cytochromes in this region. In summary, of the three redox center–bearing subunits of the ***bc*** complexes, the cytochrome ***c***–bearing component is the most variable and may have been incorporated into the complex in several different events.

CURRENT KNOWLEDGE AND FUTURE DIRECTIONS

The greatest advance in the last 5 years has been the acquisition of X-ray structural information for the vertebrate mitochondrial $\boldsymbol{bc_1}$ complex, of low resolution by crystallographic standards but sufficient for constructing detailed atomic models of the complex for the first time. In the near future we expect to see higher-resolution structures, specifying precise details of side chain and substrate and bound solvent position and orientation, and a detailed model of hydrogen bonding interactions. We also expect structures for the yeast mitochondrial complex and an α proteobacterial complex.

The X-ray structures have largely confirmed structural predictions based on lower-resolution imaging techniques, site-directed mutagenesis, and correlation of function with natural variations in sequence. The structure is consistent with the general features of the modified proton motive Q-cycle mechanism which, before any real structural information was available, was proposed to account for coupling between electron transfer and proton translocation. Details of how specific requirements of the model are met by the structure, in particular the need for enforced bifurcated electron transfer at center Q_o, were not provided. However, the structure introduced new factors that may be involved, for instance movement of the ISP, a bifurcated volume providing the possibility for two quinone binding positions in the Q_o site, and the presence of a strong hydrogen bond between the ISP cluster–binding histidine and the occupant of the Q_o site. Resolution of the details of this reaction will require functional and spectroscopic studies as well as further structural information.

A critical and more general mechanistic question that might be approached through studies of the complex is that of coupled electron and proton transfer. If the reaction at the Q_o site follows the suggested path, then it provides an opportunity for detailed spectroscopic studies in the context of a wealth of structural and physicochemical information. Similarly, the Q_i site reaction represents an additional two-electron gate that is now available for more detailed study in a structural context.

ACKNOWLEDGMENTS

The authors gratefully acknowledge funding from the NIH, grants DK44842 (to EAB) and GM35438 (to ARC). In addition, the work at LBNL was supported by the U.S. Department of Energy under Contract No. DE-AC03-76SF00098. Some of the results cited are from work done at the Stanford Synchrotron Radiation Laboratory (SSRL), which is operated by the Department of Energy, Office of Basic Energy Sciences. The SSRL Biotechnology Program is supported by the National Institutes of Health, National Center for Research Resources, Biomedical Technology Program, and by the Department of Energy, Office of Biological and Environmental Research. We want also to thank all the investigators who supplied us with preprints of papers in press or submitted, and discussed various aspects.

LITERATURE CITED

1. MacMunn CA. 1884. *J. Physiol.* 5:xxiv–xxvi
2. Keilin D. 1925. *Proc. R. Soc. London Ser. B* 98:312–39
3. Wainio WW. 1970. *The Mammalian Mitochondrial Respiratory Chain.* New York: Academic
4. Nicholls P. 1975. *Cytochromes and Biological Oxidation.* Burlington, NC: Carolina Biol. Supply. 2nd ed.
5. Rieske JS. 1976. *Biochim. Biophys. Acta* 456:195–247
6. Trumpower BL, Edwards CA. 1979. *J. Biol. Chem.* 254:8697–706
7. Hauska G, Hurt E, Gabellini N, Lockau W. 1983. *Biochim. Biophys. Acta* 726:97–133
8. Rich P. 1984. *Biochim. Biophys. Acta* 768: 53–79
9. Crofts AR. 1985. In *The Enzymes of Biological Membranes,* ed. A Martonosi, 4:347–82. New York: Plenum
10. Berry EA, Trumpower BL. 1985. In *Coenzyme Q,* ed. G Lenaz, pp. 365–89. New York: Wiley
11. Trumpower BL, Gennis RB. 1994. *Annu. Rev. Biochem.* 63:675–716
12. Brandt U, Trumpower BL. 1994. *Crit. Rev. Biochem. Mol. Biol.* 29:165–97
13. Cramer WA, Soriano GM, Ponomarev M, Huang D, Zhang H, et al.1996. *Annu. Rev. Plant Physiol. Plant Mol. Biol.* 47:477–508
14. Xia D, Yu CA, Kim H, Xia JZ, Kachurin AM, et al.1997. *Science* 277:60–66
15. Zhang ZL, Huang L-S, Shulmeister VM, Chi YI, Kim KK, et al.1998. *Nature* 392: 677–84
16. Iwata S, Lee JW, Okada K, Lee JK, Iwata M, et al. 1998. *Science* 281:64–71
17. Rieske JS, Hansen RE, Zaugg WS.1964. *J. Biol. Chem.* 239:3017–21
18. Hatefi Y, Haavik AG, Griffiths DE. 1962. *J. Biol. Chem.*. 237:1681–85
19. Rieske JS, Zaugg WS, Hansen RE. 1964. *J. Biol. Chem.* 239:3023–30
20. Rieske JS. 1967. *Methods Enzymol.* 10: 239–45
21. Yu C-A, Yu L, King TE. 1974. *J. Biol. Chem.* 249:4905–10
22. Yu C-A, Yu L. 1980. *Biochim. Biophys. Acta* 591:409–20
23. Yu C-A, Xia JZ, Kachurin AM, Yu L, Xia D, et al. 1996. *Biochim. Biophys. Acta* 1275:47–53
24. Xia D, Yu C-A, Deisenhofer J Xia J-Z, Yu L. 1996. *Biophys. J.* 70:A253

25. von Jagow G, Schagger H, Riccio P, Klingenberg M, Kolb HJ. 1977. *Biochim. Biophys. Acta* 462:549–58
26. Engel WD, Schagger H, von Jagow G. 1980. *Biochim. Biophys. Acta* 592:211–22
27. Schagger H, Link TA, Engel WD, von Jagow G. 1986. *Methods Enzymol.* 126:224–37
28. Musatov A, Robinson NC. 1994. *Biochemistry* 33:13005–12
29. Weiss H, Kolb HJ. 1979. *Eur. J. Biochem.* 99:139–49
30. Bill K, Broger C, Azzi A. 1982. *Biochim. Biophys. Acta* 679:28–34
31. Braun HP, Schmitz UK. 1992. *Eur. J. Biochem.* 208:761–67
32. Berry EA, Trumpower BL. 1985. *J. Biol. Chem.* 260:2458–67
33. Yang XH, Trumpower BL. 1986. *J. Biol. Chem.* 261:12282–89
34. Ljungdahl PO, Pennoyer JD, Robertson DE, Trumpower BL. 1987. *Biochim. Biophys. Acta* 891:227–41
35. Kriauciunas A, Yu L, Yu CA, Wynn RM, Knaff DB. 1989. *Biochim. Biophys. Acta* 976:70–76
36. Andrews KM, Crofts AR, Gennis RB. 1990. *Biochemistry* 29:2645–51
37. Robertson DE, Ding H, Chelminski PR, Slaughter C, Hsu J, et al. 1993. *Biochemistry* 32:1310–17
38. Montoya G, te Kaat K, Rodgers S, Nitschke W, Sinning I. 1999. *Eur. J. Biochem.* 259: 709–18
39. Sone N, Sekimachi M, Kutoh E. 1987. *J. Biol. Chem.* 262:15386–91
40. Kutoh E, Sone N. 1988. *J. Biol. Chem.* 263:9020–26
41. Berry EA, Huang L-S, DeRose VJ. 1991. *J. Biol. Chem.* 266:9064–77
42. Gutierrez-Cirlos EB, Antaramian A, Vazquez-Acevedo M, Coria R, Gonzalez-Halphen D. 1994. *J. Biol. Chem.* 269: 9147–54
43. Guergova-Kuras M, Salcedo-Hernandez R, Bechmann G, Kuras R, Gennis RB, Crofts AR. 1999. *Protein Expr. Purif.* 15: 370–80
44. Tian H, Yu L, Mather MW, Yu CA. 1998. *J. Biol. Chem.* 273:27953–59
45. Hurt E, Hauska G. 1981. *Eur. J. Biochem.* 117:591–95
46. Gabellini N, Bowyer JR, Hurt E, Melandri BA, Hauska G. 1982. *Eur. J. Biochem.* 126:105–11
47. Krinner MGH, Hurt E, Lockau W. 1982. *Biochim. Biophys. Acta* 681:110–17
48. Clark RD, Hind G. 1983. *J. Biol. Chem.* 258:10348–54
49. Chain RK. 1985. *FEBS Lett.* 180:321–25
50. Doyle MF, Yu CA. 1985. *Biochem. Biophys. Res. Commun.* 131:700–6
51. Black MT, Widger WR, Cramer WA. 1987. *Arch. Biochem. Biophys.* 252:655–61
52. LeMaire M, Girard-Bascou J, Wollman F-A, Bennoun P. 1986. *Biochim. Biophys. Acta* 851:229–38
53. Pierre Y, Breyton C, Kramer D, Popot J-L. 1995. *J. Biol. Chem.* 270:29342–49
54. Minami Y, Wada K, Matsubara H. 1989. *Plant Cell Physiol.* 30:91–98
55. Huang D, Zhang H, Soriano G, Dahms T, Krahn J, et al. 1998. See Ref. 288, pp. 1577–81
56. Lubben M, Kolmerer B, Saraste M. 1992. *EMBO J.* 11:805–12
57. Lubben M, Warne A, Albracht SP, Saraste M. 1994. *Mol. Microbiol.* 13:327–35
58. Lubben M, Arnaud S, Castresana J, Warne A, Albracht SP, Saraste M. 1994. *Eur. J. Biochem.* 224:151–59
59. Wingfield P, Arad T, Leonard K, Weiss H. 1979. *Nature* 280:696–97
60. Weiss H, Leonard K. 1987. *Chem. Scr.* 27B:73–81
61. Akiba T, Toyoshima C, Matsunaga T, Kawamoto M, Kubota T, et al. 1996. *Nat. Struct. Biol.* 3:553–61
62. Jungas C, Ranck JL, Rigaud JL, Joliot P, Vermeglio A. 1999. *EMBO J.* 18:534–42
63. Huang D, Everly RM, Cheng RH, Heymann JB, Schagger H, et al. 1994. *Biochemistry* 33:4401–9

64. Breyton C, Tribet C, Olive J, Dubacq JP, Popot J-L. 1997. *J. Biol. Chem.* 272: 21892–900
65. Mosser G, Breyton C, Olofsson A, Popot J-L, Rigaud JL. 1997. *J. Biol. Chem.* 272:20263–68
66. Bron P, Lacapere JJ, Breyton C, Mosser G. 1999. *J. Mol. Biol.* 287:117–26
67. Breyton C. 2000. *J. Biol. Chem.* In press
68. Schoepp B, Brugna M, Riedel A, Nitschke W, Kramer DM. 1999. *FEBS Lett.* 450: 245–50
69. Martinez SE, Huang D, Szczepaniak A, Cramer WA, Smith JL. 1994. *Structure* 2: 95–105
70. Martinez SE, Huang D, Ponomarev M, Cramer WA, Smith JL. 1996. *Protein Sci.* 5:1081–92
71. Berry E, Huang L-S, Chi Y, Zhang Z, Malkin R, Fernandez-Velasco J. 1997. *Biophys. J.* 72:A125
72. Carrell CJ, Schlarb BG, Bendall DS, Howe CJ, Cramer WA, Smith JL. 1999. *Biochemistry* 38:9590–99
73. Link TA, Saynovits M, Assmann C, Iwata S, Ohnishi T, von Jagow G. 1996. *Eur. J. Biochem.* 237:71–75
74. Iwata S, Saynovits M, Link TA, Michel H. 1996. *Structure* 4:567–79
75. Carrell CJ, Zhang H, Cramer WA, Smith JL. 1997. *Structure* 5:1613–25
76. Ozawa T, Tanaka M, Shimomura Y. 1980. *Proc. Natl. Acad. Sci. USA* 77:5084–86
77. Ozawa T, Tanaka M, Shimomura Y. 1983. *Proc. Natl. Acad. Sci. USA* 80:921–25
78. Gros P, Groendijk H, Drenth J, Hol WGJ. 1988. *J. Cryst. Growth* 90:193–200
79. Yue WH, Zou YP, Yu L, Yu CA. 1991. *Biochemistry* 30:2303–6
80. Kubota T, Kawamoto M, Fukuyama K, Shinzawa-Itoh K, Yoshikawa S, Matsubara H. 1991. *J. Mol. Biol.* 221:379–82
81. Berry EA, Huang L-S, Earnest TN, Jap BK. 1992. *J. Mol. Biol.* 224:1161–66
82. Matthews BW. 1968. *J. Mol. Biol.* 33: 491–97
83. Yu CA, Xia D, Deisenhofer J, Yu L. 1994. *J. Mol. Biol.* 243:802–5
84. Kim H, Xia D, Yu CA, Xia JZ, Kachurin AM, et al. 1998. *Proc. Natl. Acad. Sci. USA* 95:8026–33
85. von Jagow G, Ohnishi T. 1985. *FEBS Lett.* 185:311–15
86. von Jagow G, Link TA. 1986. *Methods Enzymol.* 126:253–71
87. Yoshikawa S, Shinzawa-Itoh K, Ueda H, Tsukihara T, Fukumoto YKT, et al. 1992. *J. Cryst. Growth* 122:298–302
88. Kawamoto M, Kubota T, Matsunaga T, Fukuyama K, Matsubara H, et al. 1994. *J. Mol. Biol.* 244:238–41
89. Murakami S, Shinzawa-Itoh K, Yoshikawa S. 1998. *Acta Crystallogr. Sect. D* 54:146–47
90. Berry EA, Shulmeister VM, Huang L-S, Kim S-H. 1995. *Acta Crystallogr. Sect. D* 51:235–39
91. Berry EA, Zhang Z, Huang L-S, Chi Y-I, Kim S-H. 1997. *Biophys. J.* 72:A137
92. Berry EA, Zhang Z, Huang L-S, Kim S-H. 1999. *Biochem. Soc. Trans.* 27:565–72
93. Berry EA, Huang L-S, Zhang Z, Kim S-H. 1999. *J. Bioenerg. Biomembr.* 31:177–90
94. Zhang Z-L, Berry EA, Huang L-S, Kim S-H. 2000. *Subcell. Biochem.* 36: In press
95. Lee JW, Chan M, Law TV, Kwon HJ, Jap BK. 1995. *J. Mol. Biol.* 252:15–19
96. Iwata M, Björkman J, Iwata S. 1999. *J. Bioenerg. Biomembr.* 31:169–75
97. Hunte C, Rossmanith R, Koepke J, Michel H. 1998. *EBEC Short Rep.* 10:130 (Abstr.)
98. Hunte C. 2000. *Biophys. J.* 78:v
99. Crofts AR, Guergova-Kuras M, Huang L, Kuras R, Zhang Z, Berry EA. 1999. *Biochemistry* 38:15791–806
100. Usui S, Yu L. 1991. *J. Biol. Chem.* 266: 15644–49
101. Yu L, Yu CA. 1991. *Biochemistry* 30:4934–39
102. Chen YR, Shenoy SK, Yu CA, Yu L. 1995. *J. Biol. Chem.* 270:11496–501
103. Gencic S, Schagger H, von Jagow G. 1991. *Eur. J. Biochem.* 199:123–31

104. Schagger H, Brandt U, Gencic S, von Jagow G. 1995. *Methods Enzymol.* 260: 82–96
105. Jansch L, Kruft V, Schmitz UK, Braun HP. 1995. *Eur. J. Biochem.* 228:878–85
106. Brandt U, Uribe S, Schagger H, Trumpower BL. 1994. *J. Biol. Chem.* 269: 12947–53
107. Brandt U, Yu L, Yu CA, Trumpower BL. 1993. *J. Biol. Chem.* 268:8387–90
108. Schagger H, von Jagow G. 1987. *Anal. Biochem.* 166:368–79
109. Silman HI, Rieske JS, Lipton SH, Baum H. 1967. *J. Biol. Chem.* 242:4867–75
110. Schulte U, Arretz M, Schneider H, Tropschug M, Wachter E, et al. 1989. *Nature* 339:147–49
111. Arretz M, Schneider H, Wienhues U, Neupert W. 1991. *Biomed. Biochim. Acta* 50:403–12
112. Glaser E, Sjoling S, Tanudji M, Whelan J. 1998. *Plant Mol. Biol.* 38:311–38
113. Braun HP, Schmitz UK. 1995. *Trends Biochem. Sci.* 20:171–75
114. Peiffer WE, Ingle RT, Ferguson-Miller S. 1990. *Biochemistry* 29:8696–701
115. Braun HP, Emmermann M, Kruft V, Bodicker M, Schmitz UK. 1995. *Planta* 195:396–402
116. Erikkson A, Sjöling SEG. 1994. *Biochim. Biophys. Acta* 1186:221–31
117. Priest JW, Hajduk SL. 1992. *J. Biol. Chem.* 267:20188–95
118. Marres CM, Slater EC. 1977. *Biochim. Biophys. Acta* 462:531–48
119. Chance B, Wilson DF, Dutton PL, Erecinska M. 1970. *Proc. Natl. Acad. Sci. USA* 66:1175–82
120. Dutton P, Wilson D. 1976. *Methods Enzymol.* 54:411–35
121. von Jagow G, Schagger H, Engel WD, Machleidt W, Machleidt I, Kolb HJ. 1978. *FEBS Lett.* 91:121–25
122. Wikstrom MK. 1973. *Biochim. Biophys. Acta* 301:155–93
123. Weiss H. 1976. *Biochim. Biophys. Acta* 456:291–313
124. Davis KA, Hatefi Y. 1971. *Biochem. Biophys. Res. Commun.* 44:1338–44
125. Davis KA, Hatefi Y, Poff KL, Butler WL. 1972. *Biochem. Biophys. Res. Commun.* 46:1984–90
126. Goldberger R, Smith A, Tisdale H, Bomstein R. 1961. *J. Biol. Chem.* 236:2788
127. Ohnishi K. 1966. *J. Biochem.* 59:1–8
128. Nobrega FG, Tzagoloff A. 1980. *J. Biol. Chem.* 255:9828–37
129. Anderson S, Bankier AT, Barrell BG, de Bruijn MH, Coulson AR, et al. 1981. *Nature* 290:457–65
130. Saraste M. 1984. *FEBS Lett.* 166:367–72
131. Widger WR, Cramer WA, Herrmann RG, Trebst A. 1984. *Proc. Natl. Acad. Sci. USA* 81:674–78
132. Erecinska M, Wilson DF, Blasie JK. 1978. *Biochim. Biophys. Acta* 501:63–71

132a. Degli Esposti M, Palmer G, Lenaz G. 1989. *Eur. J. Biochem.* 182:27–36

133. Colson AM, Slonimski PP. 1979. *Mol. Gen. Genet.* 167:287–98
134. Subik J, Briquet M, Goffeau A. 1981. *Eur. J. Biochem.* 119:613–18
135. Crofts A, Robinson H, Andrews K, van Doren S, Berry E. 1988. In *Cytochrome Systems,* ed. S Papa, pp. 617–24. New York: Plenum
136. Yun CH, Crofts AR, Gennis RB. 1991. *Biochemistry* 30:6747–54
137. Crofts A, Hacker B, Barquera B, Yun CH, Gennis R. 1992. *Biochim. Biophys. Acta* 1101:162–65
138. Degli Esposti M, de Vries S, Crimi M, Ghelli A, Patarnello T, Meyer A. 1993. *Biochim. Biophys. Acta* 1143:243–71
139. Gennis RB, Barquera B, Hacker B, Van Doren SR, Arnaud S, et al. 1993. *J. Bioenerg. Biomembr.* 25:195–209
140. Link TA, Wallmeier H, von Jagow G. 1994. *Biochem. Soc. Trans.* 22:197–203
141. Claros MG, Perea J, Shu Y, Samatey FA, Popot J-L, Jacq C. 1995. *Eur. J. Biochem.* 228:762–71
142. Kunz WS, Konstantinov A. 1984. *FEBS Lett.* 175:100–4

143. Glaser EG, Crofts AR. 1984. *Biochim. Biophys. Acta* 766:322–33
144. Case GD, Leigh JS Jr. 1976. *Biochem. J.* 160:769–83
145. Ohnishi T, Schagger H, Meinhardt SW, LoBrutto R, Link TA, von Jagow G. 1989. *J. Biol. Chem.* 264:735–44
146. Yakushiji E, Okunuki K. 1940. *Imp. Acad. (Tokyo)* 16:299
147. Keilin D, Hartree EF. 1940. *Proc. R. Soc. London Ser. B* 129:277
148. Wakabayashi S, Matsubara H, Kim CH, Kawai K, King TE. 1980. *Biochem. Biophys. Res. Commun.* 97:1548–54
149. Yu CA, Yu L, King TE. 1972. *J. Biol. Chem.* 247:1012–19
150. Konig BW, Schilder LT, Tervoort MJ, Van Gelder BF. 1980. *Biochim. Biophys. Acta* 621:283–95
151. Kim CH, King TE. 1981. *Biochem. Biophys. Res. Commun.* 101:607–14
152. Kim CH, King TE. 1987. *Biochemistry* 26:1955–61
153. Kim CH, King TE. 1983. *J. Biol. Chem.* 258:13543–51
154. Gonzales DH, Neupert W. 1990. *J. Bioenerg. Biomembr.* 22:753–68
155. Li Y, Leonard K, Weiss H. 1981. *Eur. J. Biochem.* 116:199–205
156. Schoepp B, Breton J, Parot P, Vermeglio A. 2000. *J. Biol. Chem.* 275:5284–90
157. Rieske JS. 1967. *Methods Enzymol.* 10: 357–62
158. Nishibayashi-Syamashita H, Cunningham C, Racker E. 1972. *J. Biol. Chem.* 247:698–704
159. Engel WD, Michalski C, von Jagow G. 1983. *Eur. J. Biochem.* 132:395–407
160. Gurbiel RJ, Batie CJ, Sivaraja M, True AE, Fee JA, et al. 1989. *Biochemistry* 28:4861–71
161. Britt RD, Sauer K, Klein MP, Knaff DB, Kriauciunas A, et al. 1991. *Biochemistry* 30:1892–901
162. Davidson E, Ohnishi T, Atta-Asafo-Adjei E, Daldal F. 1992. *Biochemistry* 31:3342–51
163. de Vries S, Albracht SP, Leeuwerik FJ. 1979. *Biochim. Biophys. Acta* 546:316–33
164. Ohnishi T, Brandt U, von Jagow G. 1988. *Eur. J. Biochem.* 176:385–89
165. Ding H, Robertson DE, Daldal F, Dutton PL. 1992. *Biochemistry* 31:3144–58
166. Li Y, De Vries S, Leonard K, Weiss H. 1981. *FEBS Lett.* 135:277–80
167. Denke E, Merbitz-Zahradnik T, Hatzfeld OM, Snyder CH, Link TA, Trumpower BL. 1998. *J. Biol. Chem.* 273:9085–93
168. Schroter T, Hatzfeld OM, Gemeinhardt S, Korn M, Friedrich T, et al. 1998. *Eur. J. Biochem.* 255:100–6
169. Crofts AR, Hong S, Ugulava N, Barquera B, Gennis R, et al. 1999. *Proc. Natl. Acad. Sci. USA* 96:10021–26
170. Hong S, Ugulava N, Guergova-Kuras M, Crofts AR. 1999. *J. Biol. Chem.* 274: 33931–44
170a. Guergova-Kuras M, Kuras R, Ugulava N, Hadad I, Crofts AR. 2000. *Biochemistry.* In press
171. Nalecz MJ, Bolli R, Azzi A. 1985. *Arch. Biochem. Biophys.* 236:619–28
172. Yu CA, Yu L. 1982. *J. Biol. Chem.* 257: 6127–31
173. Yu L, Yang FD, Yu CA. 1985. *J. Biol. Chem.* 260:963–73
174. Borchart U, Machleidt W, Schagger H, Link TA, von Jagow G. 1986. *FEBS Lett.* 200:81–86
175. Usui S, Yu L, Yu CA. 1990. *Biochemistry* 29:4618–26
176. Wang T, King TE. 1982. *Biochem. Biophys. Res. Commun.* 104:591–96
177. Wakabayashi S, Takao T, Shimonishi Y, Kuramitsu S, Matsubara H, et al. 1985. *J. Biol. Chem.* 260:337–43
178. de Haan M, van Loon AP, Kreike J, Vaessen RT, Grivell LA. 1984. *Eur. J. Biochem.* 138:169–77
179. DeLabre ML, Nett JH, Trumpower BL. 1999. *FEBS Lett.* 449:201–5

180. Schagger H, Hagen T, Roth B, Brandt U, Link TA, von Jagow G. 1990. *Eur. J. Biochem.* 190:123–30
181. Hurt E, Hauska G. 1982. *J. Bioenerg. Biomembr.* 14:405–24
182. Bertsch J, Malkin R. 1991. *Plant Mol. Biol.* 17:131–33
183. de Vitry C, Breyton C, Pierre Y, Popot J-L. 1996. *J. Biol. Chem.* 271:10667–71
184. Ketchner SL, Malkin R. 1996. *Biochim. Biophys. Acta* 1273:195–97
185. Takahashi Y, Rahire M, Breyton C, Popot J-L, Joliot P, Rochaix JD. 1996. *EMBO J.* 15:3498–506
186. Pierre Y, Breyton C, Lemoine Y, Robert B, Vernotte C, Popot J-L. 1997. *J. Biol. Chem.* 272:21901–8
187. Peterman EJ, Wenk SO, Pullerits T, Palsson LO, van Grondelle R, et al. 1998. *Biophys. J.* 75:389–98
188. Zhang H, Huang D, Cramer WA. 1999. *J. Biol. Chem.* 274:1581–87
189. Van Doren SR, Gennis RB, Barquera B, Crofts AR. 1993. *Biochemistry.* 32:8083–91
190. Kuras R, de Vitry C, Choquet Y, Girard-Bascou J, Culler D, et al. 1997. *J. Biol. Chem.* 272:32427–35
191. Yu J, Le Brun NE. 1998. *J. Biol. Chem.* 273:8860–66
192. Malkin R, Aparicio PJ, Arnon DI. 1974. *Proc. Natl. Acad. Sci. USA* 71:2362–66
193. Hurt E, Hauska G, Malkin R. 1981. *FEBS Lett.* 134:1–5
194. Szczepaniak A, Huang D, Keenan TW, Cramer WA. 1991. *EMBO J.* 10:2757–64
195. Breyton C, de Vitry C, Popot J-L. 1994. *J. Biol. Chem.* 269:7597–602
196. Prince RC, Crowder MS, Bearden AJ. 1980. *Biochim. Biophys. Acta* 592:323–37
197. Bergstrom J, Vanngard T. 1982. *Biochim. Biophys. Acta* 682:452–56
198. Riedel A, Rutherford AW, Hauska G, Muller A, Nitschke W. 1991. *J. Biol. Chem.* 266:17838–44
199. Schoepp B, Chabaud E, Breyton C, Vermeglio A, Popot J-L. 2000. *J. Biol. Chem.* 275:5275–83
200. Pearson DC Jr, Gross EL, David ES. 1996. *Biophys. J.* 71:64–76
201. Zhou J, Fernandez-Velasco JG, Malkin R. 1996. *J. Biol. Chem.* 271:6225–32
202. Soriano GM, Ponamarev MV, Piskorowski RA, Cramer WA. 1998. *Biochemistry* 37:15120–28
203. Ubbink M, Ejdeback M, Karlsson BG, Bendall DS. 1998. *Structure* 6:323–35
204. Soriano GM, Ponamarev MV, Carrell CJ, Xia D, Smith JL, Cramer WA. 1999. *J. Bioenerg. Biomembr.* 31:201–13
205. Kuras R, Wollman FA, Joliot P. 1995. *Biochemistry* 34:7468–75
206. Chi Y-I, Zhang Z, Huang L-S, Fernandez-Velasco JG, Berry E. 2000. *Biochemistry.* In press
207. Mitchell P. 1976. *J. Theor. Biol.* 62: 327–67
208. Crofts A, Wraight C. 1983. *Biochim. Biophys. Acta* 726:149–86
209. Robertson D, Dutton P. 1988. *Biochim. Biophys. Acta* 935:273–91
210. Crofts A, Wang Z. 1989. *Photosynth. Res.* 22:69–87
211. Andrews K. 1989. PhD thesis. Univ. Ill., Urbana-Champaign
212. Rieske JS. 1986. *J. Bioenerg. Biomembr.* 18:235–57
213. Matsuno-Yagi A, Hatefi Y. 1997. *J. Biol. Chem.* 272:16928–33
214. Matsuno-Yagi A, Hatefi Y. 1999. *J. Biol. Chem.* 274:9283–88
215. Junemann S, Heathcote P, Rich PR. 1998. *J. Biol. Chem.* 273:21603–7
216. Crofts AR, Meinhardt S, Jones K, Snozzi M. 1983. *Biochim. Biophys. Acta* 723:202–18
217. Meinhardt SW, Crofts AR. 1983. *Biochim. Biophys. Acta* 723:219–30
218. de Vries S, Albracht SP, Berden JA, Slater EC. 1982. *Biochim. Biophys. Acta* 681:41–53
219. Link TA. 1997. *FEBS Lett.* 412:257–64

220. Zhang L, Yu L, Yu CA. 1998. *J. Biol. Chem.* 273:33972–76
221. Skulachev VP. 1996. *Q. Rev. Biophys.* 29:169–202
222. Crofts AR, Berry EA. 1998. *Curr. Opin. Struct. Biol.* 8:501–9
223. Crofts AR, Barquera B, Gennis RB, Kuras R, Guergova-Kuras M, Berry EA. 1999. *Biochemistry* 38:15807–26
224. Ding H, Moser CC, Robertson DE, Tokito MK, Daldal F, Dutton PL. 1995. *Biochemistry* 34:15979–96
225. Ding H, Daldal F, Dutton PL. 1995. *Biochemistry* 34:15997–6003
226. Brandt U. 1996. *Biochim. Biophys. Acta* 1275:41–46
227. Brandt U. 1996. *FEBS Lett.* 387:1–6
228. Brandt U, Okun JG. 1997. *Biochemistry* 36:11234–40
229. Brandt U. 1998. *Biochim. Biophys. Acta* 1365:261–68
230. Gopta OA, Feniouk BA, Junge W, Mulkidjanian AY. 1998. *FEBS Lett.* 431: 291–96
231. Brasseur G, Saribas AS, Daldal F. 1996. *Biochim. Biophys. Acta* 1275:61–69
232. Crofts A, Barquera B, Gennis R, Kuras R, Guergova-Kuras M, Berry E. 1999. In *The Phototrophic Prokaryotes,* ed. GA Peschek, W Loeffelhardt, G Schmetterer, pp. 229–39. New York: Plenum
233. Liebl U, Sled V, Brasseur G, Ohnishi T, Daldal F. 1997. *Biochemistry* 36:11675–84
234. Brasseur G, Sled V, Liebl U, Ohnishi T, Daldal F. 1997. *Biochemistry* 36:11685–96
235. Saribas AS, Valkova-Valchanova M, Tokito MK, Zhang Z, Berry EA, Daldal F. 1998. *Biochemistry* 37:8105–14
236. Darrouzet E, Valkova-Valchanova M, Daldal F. 1998. See Ref. 288, pp. 1517–20
237. Tian H, White S, Yu L, Yu CA. 1999. *J. Biol. Chem.* 274:7146–52
238. Darrouzet E, Valkova-Valchanova M, Ohnishi T, Daldal F. 1999. *J. Bioenerg. Biomembr.* 31:275–88
239. Obungu VH, Wang Y, Amyot SM, Gocke CB, Beattie DS. 2000. *Biochim. Biophys. Acta* 1457:36–44
240. Beattie DS, Wang Y, Obungu VH. 1999. *J. Bioenerg. Biomembr.* 31:215–24
241. de Vitry C, Finazzi G, Baymann F, Kallas T. 1999. *Plant Cell* 11:2031–44
242. Crofts AR, Hong S, Zhang Z, Berry EA. 1999. *Biochemistry* 38:15827–39
243. Brugna M, Rodgers S, Schricker A, Montoya G, Kazmeier M, et al. 2000. *Proc. Natl. Acad. Sci. USA* 97:2069–74
244. Brugna M, Albouy D, Nitschke W. 1998. *J. Bacteriol.* 180:3719–23
245. Brugna M, Rodgers S, Schricker A, Montoya G, Kazmeier M, et al. 2000. *Proc. Natl. Acad. Sci. USA.* In press
246. Snyder C, Trumpower BL. 1998. *Biochim. Biophys. Acta* 1365:125–34
247. Rao BKS, Tyryshkin A, Roberts AG, Bowman MK, Kramer DM. 2000. *Biochemistry* 39:3285–86
248. Izrailev S, Crofts AR, Berry EA, Schulten K. 1999. *Biophys. J.* 77:1753–68
249. Brandt U, Schaegger H, von Jagow G. 1988. *Eur. J. Biochem.* 173:499–506
250. Sharp RE, Palmitessa A, Gibney BR, White JL, Moser CC, et al. 1999. *Biochemistry* 38:3440–46
251. Meinhardt SW, Crofts AR. 1982. *FEBS Lett.* 149:217–22
252. Bowyer JR, Dutton PL, Prince RC, Crofts AR. 1980. *Biochim. Biophys. Acta* 592:445–60
253. Matsuura K, Bowyer JR, Ohnishi T, Dutton PL. 1983. *J. Biol. Chem.* 258:1571–79
254. Sauter H, Ammermann E, Roehl F. 1996. In *Crop Protection Agents from Nature,* ed. LG Copping, pp. 50–81. Cambridge, UK: R. Soc. Chem./Thomas Graham House
255. Link TA, Haase U, Brandt U, von Jagow G. 1993. *J. Bioenerg. Biomembr.* 25:221–32
256. Saribas AS, Ding H, Dutton PL, Daldal F. 1997. *Biochim. Biophys. Acta* 1319: 99–108

257. Fato R, Cavazzoni M, Castelluccio C, Castelli GP, Palmer G, et al. 1993. *Biochem. J.* 290:225–36
258. Crofts A, Berry E, Kuras R, Guergova-Kuras M, Hong S, Ugulava N. 1998. See Ref. 288, pp. 1481–86
259. Moser CC, Page CC, Farid R, Dutton PL. 1995. *J. Bioenerg. Biomembr.* 27:263–74
260. Link T. 1994. *Biochim. Biophys. Acta* 1185:81–84
261. Ugulava NB, Crofts AR. 1998. *FEBS Lett.* 440:409–13
262. Deleted in proof
263. Ponamarev MV, Cramer WA. 1998. *Biochemistry* 37:17199–208
264. Kramer DM, Crofts AR. 1993. *Biochim. Biophys. Acta* 1183:72–84
265. Kramer DM, Crofts AR. 1993. *Biochim. Biophys. Acta* 1184:193–201
266. Kramer DM, Joliot A, Joliot P, Crofts AR. 1993. *Biochim. Biophys. Acta* 1184: 251–62
267. Gray KA, Dutton PL, Daldal F. 1994. *Biochemistry* 33:723–33
268. Hacker B, Barquera B, Crofts AR, Gennis RB. 1993. *Biochemistry* 32:4403–10
269. Hacker B, Barquera B, Gennis RB, Crofts AR. 1994. *Biochemistry* 33:13022–31
270. Glaser EG, Meinhardt SW, Crofts AR. 1984. *FEBS Lett.* 178:336–42
271. Robertson DE, Prince RC, Bowyer JR, Matsuura K, Dutton PL, Ohnishi T. 1984. *J. Biol. Chem.* 259:1758–63
272. Meinhardt S, Crofts A. 1984. In *Advances in Photosynthesis Research,* ed. C Sybesma, 1:649–52. The Hague: Martinus Nijhoff/Dr W Junk
273. Salerno JC, Xu Y, Osgood MP, Kim CH, King TE. 1989. *J. Biol. Chem.* 264: 15398–403
274. Rich PR, Jeal AE, Madgwick SA, Moody AJ. 1990. *Biochim. Biophys. Acta* 1018:29–40
275. Crofts AR, Barquera B, Bechmann G, Guergova M, Salcedo-Hernandez R, et al. 1995. In *Photosynthesis: From Light to Biosphere,* ed. P Mathis, 2:493–500. Dordrecht, Netherlands: Kluwer Acad.
276. Siedow JN, Power S, de la Rosa FF, Palmer G. 1978. *J. Biol. Chem.* 253:2392–99
277. de la Rosa FF, Palmer G. 1983. *FEBS Lett.* 163:140–43
278. Bechmann G, Weiss H, Rich PR. 1992. *Eur. J. Biochem.* 208:315–25
279. Hauska G, Nitschke W, Herrmann RG. 1988. *J. Bioenerg. Biomembr.* 20:211–28
280. Dandekar T, Snel B, Huynen M, Bork P. 1998. *Trends Biochem. Sci.* 23:324–28
281. Oh-oka H, Iwaki M, Itoh S. 1998. *Biochemistry* 37:12293–300
282. Juretic D, Lucin A. 1998. *J. Chem. Inf. Comput. Sci.* 38:575–85
283. Lake JA, Moore JE. 1998. *Trends Biotechnol. (S)*:22–23
284. Duneau JP, Genest D, Genest M. 1996. *J. Biomol. Struct. Dyn.* 13:753–69
285. Zito F, Finazzi G, Joliot P, Wollman FA. 1998. *Biochemistry* 37:10395–403
286. Xiong J, Inoue K, Bauer CE. 1998. *Proc. Natl. Acad. Sci. USA* 95:14851–56
287. Gonzalez-Halphen D, Vazquez-Acevedo M, Garcia-Ponce B. 1991. *J. Biol. Chem.* 266:3870–76
288. Garab G, ed. 1998. *Photosynthesis: Mechanisms and Effects,* Vol. 3. Dordrecht, Netherlands: Kluwer Acad.